

We thank the editor for the comments. The discussion about the fraction of H<sub>2</sub> removal within soil will be added to the manuscript, and the front size of Fig. 6 will be changed accordingly.

**Comments from the editor:**

Thank you for your revised submission, which I will be happy to accept for publication in ACP, subject to the following minor revisions:

- You have addressed the missing quantification of the term "large fraction" (as highlighted by referee #2) in the author's response, but not in the final manuscript. As you say, the term is subject to uncertainties, but your response shows that these are quantifiable, so please include your considerations in a revised manuscript.
- Please increase the size of axis labels and legends to at least 10 point when resized to their final width (8 or 16 cm, depending on whether they will be one or two columns wide).

**Response and changes in the manuscript:** The front size of Fig. 6 has been changed accordingly in the new manuscript. In addition, we have added the discussion about the fraction of H<sub>2</sub> removal within soil from Line 691 to Line 708.

1    **Isotopic signatures of production and uptake of H<sub>2</sub> by soil**

2

3    Qianjie Chen<sup>1,2</sup>, Maria E Popa<sup>1</sup>, Anneke M Batenburg<sup>1,3</sup>, and Thomas Röckmann<sup>1</sup>

4

5    <sup>1</sup> Institute for Marine and Atmospheric research Utrecht, Utrecht University, The Netherlands

6    <sup>2</sup> Department of Atmospheric Sciences, University of Washington, Seattle, Washington, USA

7    <sup>3</sup> Department of Applied Physics, University of Eastern Finland, Kuopio, Finland

8

9

10

11

12

13

14

15

16

17

18

19

20

21

22

**Abstract:** Molecular hydrogen ( $H_2$ ) is the second most abundant reduced trace gas (after methane) in the atmosphere, but its biogeochemical cycle is not well understood. Our study focuses on the soil production and uptake of  $H_2$  and the associated isotope effects. Air samples from a grass field and a forest site in the Netherlands were collected using soil chambers. The results show that uptake and emission of  $H_2$  occurred simultaneously at all sampling sites, with strongest emission at the grassland sites where clover ( $N_2$  fixing legume) was present. The  $H_2$  mole fraction and deuterium content were measured in the laboratory to determine the isotopic fractionation factor during  $H_2$  soil uptake ( $\alpha_{soil}$ ) and the isotopic signature of  $H_2$  that is simultaneously emitted from the soil ( $\delta D_{soil}$ ). By considering all net-uptake experiments, an overall fractionation factor for deposition of  $\alpha_{soil} = k_{HD} / k_{HH} = 0.945 \pm 0.004$  (95% CI) was obtained. The difference in mean  $\alpha_{soil}$  between the forest soil  $0.937 \pm 0.008$  and the grassland  $0.951 \pm 0.025$  is not statistically significant. For two experiments, the removal of soil cover increased the deposition velocity ( $v_d$ ) and  $\alpha_{soil}$  simultaneously, but a general positive correlation between  $v_d$  and  $\alpha_{soil}$  was not found in this study. When the data are evaluated with a model of simultaneous production and uptake, the isotopic composition of  $H_2$  that is emitted at the grassland site is calculated as  $\delta D_{soil} = (-530 \pm 40) \text{‰}$ . This is less deuterium-depleted than what is expected from isotope equilibrium between  $H_2O$  and  $H_2$ .

43

## 44 1. Introduction

45

46 H<sub>2</sub> is considered as alternative energy carrier to replace fossil fuels in the future.

47 However, the environmental and climate impact of a potential widespread use

48 of H<sub>2</sub> is still under assessment. Several studies suggested that the atmospheric

49 H<sub>2</sub> mole fraction might increase substantially in the future due to the leakage

50 during production, storage, transportation and use of H<sub>2</sub>, which could

51 significantly affect atmospheric chemistry (Schultz et al., 2003; Tromp et al.,

52 2003; van Ruijven et al., 2011; Warwick et al., 2004).

53

54 In the troposphere, H<sub>2</sub> has a mole fraction of about 550 parts per billion (ppb =

55 nmol mol<sup>-1</sup>) and a lifetime of around 2 years (Novelli et al., 1999; Price et al.,

56 2007; Xiao et al., 2007; Pieterse et al., 2011; 2013). H<sub>2</sub> can affect atmospheric

57 chemistry and composition in several ways. Firstly, it increases the lifetime of

58 the greenhouse gas methane (CH<sub>4</sub>) via its competing reaction with the hydroxyl

59 radical (OH) (Schultz et al., 2003; Warwick et al., 2004). Additionally, H<sub>2</sub>

60 affects air quality because it is an ozone (O<sub>3</sub>) precursor and indirectly increases

61 the lifetime of the air pollutant carbon monoxide (CO) through competition for

62 OH. In the stratosphere, H<sub>2</sub>O that is produced through the oxidation of H<sub>2</sub>

63 increases humidity, which can result in increased formation of polar



64 stratospheric clouds and O<sub>3</sub> depletion (Tromp, et al., 2003), but this effect may  
65 be weaker than estimated initially (Warwick et al. 2004; Vogel et al., 2012).

66

67 The main sources of tropospheric H<sub>2</sub> are the oxidation of CH<sub>4</sub> and non-methane  
68 hydrocarbons (NMHC) (48%), biomass burning (19%), fossil fuel combustion  
69 (22%) and biogenic N<sub>2</sub> fixation in the ocean (6%) and on land (4%), while the  
70 main sinks are soil uptake (70%) and oxidation by OH (30%) (Pieterse et al,  
71 2013).

72

73 The biogenic soil sink of H<sub>2</sub> is the largest and most uncertain term in the global  
74 atmospheric H<sub>2</sub> budget. Conrad and Seiler (1981) assumed that the soil uptake  
75 of atmospheric H<sub>2</sub> is most likely due to consumption by abiotic enzymes, since  
76 there were no soil microorganisms known to be able to fix H<sub>2</sub> at the low  
77 atmospheric mole fraction at that time. This remained the basic hypothesis of  
78 many further soil uptake studies (Conrad et al., 1983; Conrad and Seiler, 1985;  
79 Ehhalt and Rohrer, 2011; Guo and Conrad, 2008; Häring et al., 1994; Smith-  
80 Downey et al., 2006). However, Constant et al. (2008a) were first to identify an  
81 aerobic microorganism (*Streptomyces* sp. PCB7) that can consume H<sub>2</sub> at  
82 tropospheric ambient mole fractions, and suggested that active metabolic cells  
83 could be responsible for the soil uptake of H<sub>2</sub> rather than extracellular enzymes.  
84 Further studies showed that uptake activity at ambient H<sub>2</sub> level is widespread  
85 among the streptomycetes (Constant et al., 2010) and it was postulated that high

86 affinity  $H_2$ -oxidizing bacteria are the main biological agent responsible for the  
87 soil uptake of atmospheric  $H_2$  (Constant et al., 2011). Khdhiri et al. (2015)  
88 suggested that the relative abundance of high affinity  $H_2$ -oxidation bacteria and  
89 soil carbon content could be used as predictive parameters for the  $H_2$  oxidation  
90 rate. Determining the dominant mechanism of the  $H_2$  soil uptake activity is still  
91 an active area of research.

92  
93 It has been shown that soil uptake of  $H_2$  can coexist with soil production  
94 (Conrad, 1994).  $H_2$  is produced in the soil during  $N_2$  fixation (e.g. by bacteria  
95 living symbiotically in the roots of legumes such as clover or beans) and dark  
96 fermentation. Although the  $H_2$  produced in the soil by e.g.  $N_2$  fixation can be  
97 largely consumed within the soil, a significant amount of  $H_2$  escapes to the  
98 atmosphere (Conrad and Seiler, 1979; 1980). Conrad and Seiler (1980)  
99 estimated that 2.4 to 4.9 Tg  $a^{-1}$  of  $H_2$  is emitted into the atmosphere through  $N_2$   
100 fixation on land.

101  
102 One approach to better understand the sources and sinks of  $H_2$  is to investigate  
103 the isotopic fractionation processes involved, which act as a fingerprint for  $H_2$   
104 emitted from different sources or destroyed by different sinks. The isotopic  
105 composition of  $H_2$  is expressed as:

106

$$\delta(\text{D}, \text{H}_2) = \frac{R_{\text{sa}}}{R_{\text{VSMOW}}} - 1$$

107

108 where  $R_{\text{sa}}$  is the D/H ratio of the sample  $\text{H}_2$  and  $R_{\text{VSMOW}} = (155.76 \pm 0.8)$  parts per  
 109 million ( $\text{ppm} = \text{mmol mol}^{-1}$ ) is the same ratio of the standard material, Vienna  
 110 Standard Mean Ocean Water (VSMOW) (De Wit et al., 1980; Gonfiantini et al.,  
 111 1993). For brevity, we will use the notation  $\delta\text{D}$  ( $=\delta\text{D}(\text{D}, \text{H}_2)$ ) throughout the  
 112 rest of this paper. The  $\delta\text{D}$  values are usually given in per mill ( $\text{‰}$ ). Recent  
 113 studies showed that the global mean  $\delta\text{D}$  value of atmospheric  $\text{H}_2$  is about  $+130 \text{ ‰}$   
 114 (Batenburg et al., 2011; Gerst et al., 2000, 2001; Rice et al., 2010).

115

116 The  $\text{HH}$  molecule is consumed preferentially over  $\text{HD}$  during both  $\text{OH}$   
 117 oxidation and soil uptake, with  $\text{OH}$  oxidation causing a much stronger isotope  
 118 fractionation effect. Only a few studies have investigated the soil uptake of  $\text{H}_2$   
 119 with isotope techniques. Gerst and Quay (2001) carried out field experiments in  
 120 Seattle, United States and found  $\alpha_{\text{soil}} (= k_{\text{HD}}/k_{\text{HH}})$  to be  $0.943 \pm 0.024$  ( $1\sigma$ ). Note  
 121 that  $k_{\text{HD}}$  and  $k_{\text{HH}}$  are removal rate constants for  $\text{HD}$  and  $\text{HH}$  respectively. Rahn  
 122 et al. (2002a) collected air samples from four forest sites in ecosystems of  
 123 different ages in Alaska, United States, in July 2001, and obtained a similar  
 124 average value ( $0.94 \pm 0.01$ ). They suggested that  $\alpha_{\text{soil}}$  depends on the forest  
 125 maturity, with smaller fractionation for more mature forests. Since the more  
 126 mature forests showed larger deposition velocity ( $v_d$ ) of  $\text{H}_2$ , they further

127 suggested that lower uptake rates involve greater isotopic fractionation ( $\alpha_{\text{soil}}$   
 128 further from 1) than fast uptake rates. Rice et al. (2011) performed deposition  
 129 experiments in Seattle and found  $\alpha_{\text{soil}}$  varying from 0.891 to 0.976, with a mean  
 130 of 0.934. They found  $\alpha_{\text{soil}}$  to be correlated with  $v_d$ , with smaller isotope effects  
 131 ( $\alpha_{\text{soil}}$  closer to 1) occurring at higher  $v_d$ , which agreed with the suggestion by  
 132 Rahn et al. (2002a). In addition, unpublished experiments from Rahn et al.  
 133 (2005) yielded  $\alpha_{\text{soil}} = 0.89 \pm 0.03$  in three upland ecosystems that were part of an  
 134 Alaskan fire chronosequence. The data suggest that variability in the  
 135 soil/ecosystem affects  $\alpha_{\text{soil}}$  but no significant variability of  $\alpha_{\text{soil}}$  with season was  
 136 detected. Hitherto, only  $\alpha_{\text{soil}}$  values from studies in Seattle and Alaska are  
 137 available, and values from other locations and ecosystems are needed to learn  
 138 more about the factors influencing  $\alpha_{\text{soil}}$ .

139

140 The  $\delta D$  of  $H_2$  from various surface sources has been reported as about -290 ‰  
 141 for biomass burning (Gerst and Quay, 2001; Haumann et al., 2013) and between  
 142 -200 ‰ and -360 ‰ for fossil fuels combustion (Rahn et al., 2002b; Vollmer et  
 143 al., 2012). So far no field studies have determined the isotopic composition of  
 144 the  $H_2$  emitted from soil. Two laboratory studies examined the isotopic  
 145 signature of  $H_2$  produced from  $N_2$  fixation. Luo et al. (1991) reported a  
 146 fractionation factor  $\alpha_{H_2/H_2O} = R(D/H, H_2)/R(D/H, H_2O) = 0.448 \pm 0.001$  between  
 147 the  $H_2$  produced from  $N_2$  fixation and the  $H_2O$  used to grow the  $N_2$ -fixing  
 148 bacteria for *Synechococcus sp.* and  $0.401 \pm 0.002$  for *Anabaena sp.*, respectively.

149 Walter et al. (2012) reported  $\alpha_{\text{H}_2/\text{H}_2\text{O}} = 0.363 \pm 0.019$  for the  $\text{N}_2$ -fixing  
150 rhizobacterium *Azospirillum brasiliensis*. It has been proposed that  
151 microbiological  $\text{H}_2$  consumption and production could modify the thermal  
152 isotopic equilibrium between  $\text{H}_2$  and  $\text{H}_2\text{O}$  in low-temperature hydrothermal  
153 fluids (Kawagucci et al., 2010). Compared to the surface sources,  $\text{H}_2$  produced  
154 from  $\text{CH}_4$  and NMHC oxidation is isotopically strongly enriched in deuterium,  
155 with  $\delta\text{D}$  between +120 and +180 ‰ (Rahn et al., 2003; Röckmann et al. 2003a,  
156 Pieterse et al., 2011).

157

158 Here we report measurements of the isotopic fractionation factors of  $\text{H}_2$  during  
159 soil deposition at two different sites in the Netherlands, a forest and a grassland  
160 site. For the grassland site we also determine the apparent isotopic composition  
161 of the  $\text{H}_2$  that was simultaneously emitted from the soil during the experiment.

162

163

## 164 **2. Methods**

165

### 166 **2.1 Sampling**

167

168 Air samples were collected from a soil chamber at two locations in the  
169 Netherlands (Fig. 1): a grass field around the Cabauw tall tower (51°58' N,

170 4°55' E) and a forest site near Speuld (52°13' N, 5°39' E). Two types of ground  
171 cover (grass with and without clover) were sampled at Cabauw, while three  
172 types of forest (Douglas fir, beech and spruce) were selected in Speuld. More  
173 information about the soil and vegetation type can be found in Beljaars and  
174 Bosveld (1997) for the Cabauw site, and in Heij and Erisman (1997) for the  
175 Speuld site.

176

177 Flask samples were filled with air from a soil chamber, using a closed-cycle air  
178 sampler (Fig. 2). The soil chamber consisted of two parts: the chamber body  
179 with a metal base at the bottom that was inserted about 2 cm into the soil, and a  
180 removable transparent lid with two connections for air sampling. The chamber  
181 had a height of 40 cm, an area of 570 cm<sup>2</sup> and a volume of 22.8 L; the air inside  
182 was mixed by a fan. The sampler could hold four flasks installed in series,  
183 which could be bypassed independently; the flow and pressure in the flasks  
184 were controlled. The air was dried using Mg(ClO<sub>4</sub>)<sub>2</sub>. After passing through the  
185 flasks the air was returned to the soil chamber, which kept the pressure inside  
186 the chamber approximately constant during sampling.

187

188 Air samples were collected from the chamber in 1 L glass flasks at 0, 10, 20 and  
189 30 minutes after closing the chamber (time interval changed to 5 minutes in  
190 Speuld because of the faster uptake). The gas flasks (Normag, Ilmenau,  
191 Germany) were made of borosilicate glass 3.3 with O-ring-sealed stopcocks

192 made of PCTFE (Kel-F) and covered with a dark hose. Thorough tests have  
193 demonstrated that air samples with typical trace gas content are stable in these  
194 flasks (Rothe et al., 2004). In the beginning, the whole sampling unit (all lines,  
195 connections and flasks) was flushed with ambient air for about 10 minutes at a  
196 flow rate of 2 L min<sup>-1</sup> and a pressure of 100 kPa, with all flasks open and the  
197 chamber lid open. This initial flushing process was designed to fill the flasks  
198 with background air. The air pressure inside the flasks was increased to 200 kPa  
199 (180 kPa for Speuld samples) by adjusting the flow control valve and the valves  
200 on two pressure gauges (Fig. 2) before chamber closing and then maintained  
201 constant during the whole sampling time. The flow rate was maintained at 2 L  
202 min<sup>-1</sup> at ambient pressure and temperature with a rotameter and the pressure  
203 inside the chamber was maintained at 100 kPa during the whole sampling time.  
204 The temperature was not recorded during the sampling. After the initial flushing,  
205 the first flask was closed and then the chamber was closed as well. Afterwards,  
206 the air was flushed from the chamber through three flasks (the first flask was  
207 by-passed) and back to the chamber. After 10, 20 and 30 minutes, the second,  
208 third and fourth flasks were closed.

209

210 A total of 36 sets of air samples were collected in Cabauw during summer (June,  
211 July and August) 2012 and 12 sets were collected in Speuld in September 2012.  
212 Each set contains four air samples. In total, 186 valid samples were analyzed for  
213 H<sub>2</sub> mole fraction and its deuterium content (6 were lost during sampling,

214 transportation and measurement). All the Speuld samples and about half of the  
215 Cabauw samples were further used for analysis in this study. The reason why 50%  
216 of the Cabauw experiments were not used is that these experiments showed  
217 neither strong H<sub>2</sub> emission nor H<sub>2</sub> uptake and the isotopic signals were weak.  
218 Most experiments were conducted with the 22.8 L volume soil chamber as  
219 described above, while 10 experiments were conducted with a larger automated  
220 soil chamber with a volume of 125 L and a height of 22.5 cm.

221

222

## 223 **2.2 Laboratory determination of H<sub>2</sub> mole fraction and deuterium**

### 224 **content of air samples**

225

226 The mole fraction and the  $\delta D$  of H<sub>2</sub> were measured with a gas chromatography  
227 isotope ratio mass spectrometry (GC/IRMS) setup (Rhee et al., 2004). For H<sub>2</sub>  
228 mole fractions, the laboratory working standards are linked to the MPI-2009  
229 scale (Jordan and Steinberg, 2011). The  $\delta D$  values of the laboratory reference  
230 gases are indirectly linked to mixtures of synthetic air with H<sub>2</sub> of known  
231 isotopic composition, certified by Messer Griesheim, Germany (Batenburg et al.,  
232 2011). Most of the samples collected from Cabauw were measured within two  
233 months after sampling, while the samples from Speuld were kept in a dark  
234 storage room for around four months before measurement.



235

236 The operational principle of the GC/IRMS system is to separate H<sub>2</sub> from the air  
237 matrix at low temperature (about 36 K) and measure the HH and HD content  
238 with a mass spectrometer. The measurement includes four main steps:

239

240 (1) A glass sample volume (750 ml) is evacuated and subsequently filled with  
241 sample air to approximately 700 mbar. This volume is then exposed to a cold  
242 head (36 K) of a closed-cycle helium compressor for 9 minutes. During this  
243 stage, all gases except H<sub>2</sub>, helium (He) and neon (Ne) condense.

244

245 (2) The remainder in the headspace of the cold head and sample volume is then  
246 flushed with He carrier gas to a pre-concentration trap where H<sub>2</sub> is collected on  
247 a 25 cm long, 1/8 inch OD (outside diameter) stainless steel tube filled with fine  
248 grains (0.2 to 0.5 mm) of 5 Å molecular sieve, for 20 minutes. The pre-  
249 concentration trap is cooled down to the triple point of nitrogen (63 K) by  
250 keeping it in a liquid N<sub>2</sub> reservoir that is further cooled down by pumping on the  
251 gas phase.

252

253 (3) After the collection of H<sub>2</sub>, the pre-concentration trap is warmed up to release  
254 the absorbed H<sub>2</sub>, which is then cryo-focused for 4 minutes on a capillary (25 cm  
255 long, 0.32 mm ID (inside diameter)) filled with 5 Å molecular sieve at 77 K.  
256 After that, the cryo-focus trap is warmed up to ambient temperature and the H<sub>2</sub>

sample is flushed with He carrier gas onto the GC column (5 Å molecular sieve,  
≈323 K) where H<sub>2</sub> is chromatographically purified from potential remaining  
interferences.

260

(4) In the end, the purified H<sub>2</sub> is carried by the He carrier gas via an open split  
interface (Röckmann et al., 2003b) into the IRMS for D/H ratio determination.

263

More details about the GC/IRMS system and measurement steps can be found  
in Rhee et al. (2004) and Röckmann et al. (2010). The data correction  
procedures and isotope calibration are similar to those described in Batenburg et  
al. (2011). Four reference gases were used to determine the δD values of the  
samples. Two of them (Ref-1 and Ref-2) with δD values of (+207.0 ± 0.3) ‰  
and (+198.2 ± 0.5) ‰ were calibrated and used previously in Batenburg et al.  
(2011). The other two new reference gases (Ref-3 and Ref-4) were calibrated  
versus Ref-1 and Ref-2. The δD value of Ref-3 was (-183 ± 2.4) ‰. Ref-4 was a  
frequently measured reference gas that was measured usually about 5 times per  
sequence of measurement, while other three reference gases were measured  
about 1 to 3 times per sequence of measurement. The δD value of Ref-4  
dropped linearly with time from -115 ‰ to -157 ‰ between 1 Jun 2012 and 15  
Feb 2013, while the other three reference gases were stable.

277

## 2.3 Non-linearity of the GC/IRMS system

Ideally, the  $\delta D$  of  $H_2$  measured with the GC/IRMS should not depend on the total amount of  $H_2$  used for analysis, but in practice a dependence of the isotopic composition on the amount of  $H_2$  is observed for low mole fractions. This is called non-linear behavior, and it is a particularly severe limitation for soil uptake studies, since the mole fraction in such samples can decrease by more than an order of magnitude. For comparison, in ambient background air the  $H_2$  mole fraction variations are usually no more than 20%.

Experiments were carried out with different quantities of air from various laboratory reference bottles with known  $\delta D$  to determine a suitable correction for the non-linear behavior. The measured  $\delta D$  increases with the mass 2 sample peak area, which is proportional to the  $H_2$  quantity in the sample. In the peak area range of 0.2 Vs to 1 Vs this relation can be parameterized by a logarithmic function  $\delta D = 54.6 \ln (\text{peak area}/V_s) \text{ ‰}$ , which is used as correction function for the measurements at low peak areas (Fig. 3). The linearity correction introduces an additional uncertainty due to uncertainties in the logarithmic fit, particularly at low peak areas. The total assigned uncertainty for each measurement is calculated from the analytical and fitting uncertainty, as a function of peak area (Fig. 4). It is 2 ‰ for  $\ln (\text{peak area}/V_s)$  of 1.5 or more

299 (equivalent to more than 600 ppb H<sub>2</sub> in an air sample), but increases to 32 ‰  
300 when ln (peak area/Vs) drops to -1.6 (≈ 20 ppb H<sub>2</sub> in air sample). In total, the  
301 δD results of 18 Speuld samples that were measured at these low peak areas  
302 were corrected with this linearity correction. Possible additional systematic  
303 errors (a few ‰) may arise from uncertainties in the initially assigned δD  
304 values of the commercial calibration gases, changes of these values in the  
305 process of creating calibration mixtures with near-ambient H<sub>2</sub> concentration,  
306 and the calibration measurements themselves (Batenburg et al., 2011).

307

308

## 309 **2.4 Data evaluation**

310

311 Assuming first order kinetics for H<sub>2</sub> removal and a constant production rate  $P$   
312 over the course of a deposition experiment, the time evolution of the mole  
313 fraction  $c$  of non-deuterated H<sub>2</sub> (HH) inside the soil chamber can be expressed  
314 as:

315

$$\frac{dc}{dt} = P - kc \quad (1)$$

316

317 where  $k$  is the first order uptake rate constant of HH. For well-mixed air in the  
318 chamber,  $k = v_d/h$ , where  $v_d$  is the gross deposition velocity of H<sub>2</sub> and  $h$  is the

319 chamber height. The gross deposition velocity is the deposition velocity  
 320 corrected for production, which is different from the net deposition velocity  
 321 reported in some studies in the past that showed the effective uptake of H<sub>2</sub> from  
 322 the atmosphere. The solution of Eq. (1) is of the form:

323

$$c = (c_i - c_e)e^{-kt} + c_e \quad (2)$$

324

325 where  $c$ ,  $c_i$  and  $c_e (= P/k)$  are the mole fractions of HH at time  $t$ , initially and at  
 326 equilibrium, respectively. Therefore,  $P$  and  $k$  can be obtained by fitting an  
 327 exponential function to the time evolution of HH inside the chamber. Similarly,  
 328 we can obtain  $P'$  and  $k'$  from the time evolution of HD.

329

$$c' = (c'_i - c'_e)e^{-k't} + c'_e \quad (3)$$

330

331 where  $c'$ ,  $c'_i$ ,  $c'_e (= P'/k')$ ,  $P'$  and  $k'$  are the corresponding parameters for HD.

332

333 Equations (2) and (3) constitute the mass balance model that we used to analyze  
 334 our data. When  $k$ ,  $k'$ ,  $P$  and  $P'$  have been determined,  $\alpha_{\text{soil}}$  and  $\delta D_{\text{soil}}$  can be  
 335 calculated simply as:

336

$$\alpha_{\text{soil}} = \frac{k'}{k} \quad (4)$$

337

$$\delta D_{\text{soil}} = \frac{P'/P}{2R_{\text{VSMOW}}} - 1 \quad (5)$$

338

339 However, fitting an exponential curve to only four sample data yields relatively  
 340 large errors for  $k$ ,  $k'$ ,  $P$  and  $P'$ , which propagate to large errors for  $\alpha_{\text{soil}}$  and  $\delta D_{\text{soil}}$   
 341 if they are determined directly from Eqs (4-5).

342

343 In Rice et al. (2011), Equations (2) and (3) were combined to calculate  $\alpha_{\text{soil}}$  in  
 344 the presence of both source and sink of  $H_2$  using  $c_e$  and  $c_e'$  from the exponential  
 345 fits:

346

$$\ln \frac{c' - c_e'}{c_i' - c_e'} = \frac{k'}{k} \ln \frac{c - c_e}{c_i - c_e} \quad (6)$$

347

348  $\alpha_{\text{soil}} = k'/k$  can be obtained by plotting  $\ln \frac{c' - c_e'}{c_i' - c_e'}$  versus  $\ln \frac{c - c_e}{c_i - c_e}$  and fitting a linear  
 349 function. In the absence of soil emission ( $c_e = c_e' = 0$ ), Eq. (6) collapses to the  
 350 well-known Rayleigh fractionation equation that is used to quantify the isotope  
 351 fractionation during single stage removal processes in the absence of sources.

352

353 For the high emission measurements, where production overwhelms  
354 consumption, we use the relations  $c_e = P/k$  and  $c'_e = P'/k'$ , and obtain  $P'/P$  from  
355 the slope of  $c'_e \ln \frac{c'_i - c'_e}{c'_i - c'_e}$  against  $c_e \ln \frac{c - c_e}{c_i - c_e}$ . Then  $\delta D_{\text{soil}}$  is calculated from Eq. (5).

356

## 357 **2.5 Flask sampling model**

358

359 The advantage of sampling with the soil chamber system described in Section  
360 2.1 was that the pressure in the soil chamber stayed constant even when several  
361 large samples (2 L each) were taken. A disadvantage was that the volume of air  
362 inside the flasks (8 L of air in total) was considerable compared to the volume  
363 of air inside the soil chamber (22.8 L). This had two effects: (1) A significant  
364 part of the air was at each time separated from the chamber and thus from the  
365 soil production and uptake. (2) Because of the time lag to flush the samples, the  
366 air in a flask was not the same as the air in the chamber at the same time.

367

368 We built a flask sampling model to derive correction factors that take into  
369 account the influence of the flask sampling system. For a given combination of  
370 uptake and production rates, the model simulates the evolution of the  $H_2$  mole  
371 fraction in two configurations: the soil chamber alone, and the soil chamber plus  
372 four flasks as in our experiments. The model is described in detail in Appendix  
373 A. An example of a simulation is shown in Fig. 5. Compared to the situation

374 without flasks, there is a time lag in the decay of  $H_2$  for both the chamber and  
375 the flasks after introducing four flasks in the model. The time lag for the second  
376 flask is about 2.5 minutes. It increases to 5 minutes for the third flask and is  
377 even longer for the fourth flask.

378

379 It is obvious that the sampling process strongly affects the uptake rate  $k_{app}$  and  
380 production rate  $P_{app}$  obtained from the direct flask measurements, so we  
381 corrected all  $k_{app}$  and  $P_{app}$  values with the correction coefficients derived from  
382 this flask sampling model (Appendix A). For a fixed chamber volume, sample  
383 pressure, flow rate and time interval of the flask collection that are all recorded  
384 for each experiment, the relationship between the actual uptake rate constant  
385  $k_{true}$  and apparent uptake rate constant  $k_{app}$  can be obtained (see Appendix A).  
386 Under the same sampling conditions for a fixed value of  $P_{app}$ , the relationship  
387 between actual production rate  $P_{true}$  and apparent production rate  $P_{app}$  depends  
388 on  $k_{true}$  (Fig 10b).

389

390 To evaluate the data, we first applied an exponential fit as in Eq. (2) to the  
391 measured HH mole fractions for the four flasks in each experiment and obtained  
392 *apparent* values  $k_{app}$ ,  $P_{app}$  and  $c_{e,app}$  from the fit parameters. Then we used the  
393 correction factors derived from the flask sampling model to retrieve true values



394  $k_{\text{true}}$  and  $P_{\text{true}}$  from the apparent values  $k_{\text{app}}$  and  $P_{\text{app}}$ . One can obtain  $k'_{\text{true}}$  and  $P'_{\text{true}}$   
395 by applying the same method to HD mole fractions inside four flasks.

396

397 To determine  $\alpha_{\text{soil}}$ , we plotted  $\ln \frac{c' - c'_{\text{e,app}}}{c'_1 - c'_{\text{e,app}}}$  versus  $\ln \frac{c - c_{\text{e,app}}}{c_1 - c_{\text{e,app}}}$  (Eq.6, Fig. 7) and  
398 obtained  $\alpha_{\text{soil,app}}$  from the slope of the linear regression. Here,  $c$  and  $c'$  are HH  
399 and HD mole fractions in each of the four flasks;  $c_1$  and  $c'_1$  are HH and HD  
400 mole fractions of the first flask;  $c_{\text{e,app}}$  and  $c'_{\text{e,app}}$  are apparent HH and HD  
401 equilibrium mole fractions obtained from the exponential fits of HH and HD  
402 mole fractions inside the four flasks. We determined the relationship (Fig. 10c)  
403 between  $\alpha_{\text{soil,true}}$  and  $\alpha_{\text{soil,app}}$  obtained from  $\ln \frac{c' - c'_{\text{e,app}}}{c'_1 - c'_{\text{e,app}}}$  versus  $\ln \frac{c - c_{\text{e,app}}}{c_1 - c_{\text{e,app}}}$  using the  
404 flask sampling model (see Appendix A1.3). The correction coefficients for each  
405 experiment are given in Table 3.

406

407 Similarly, we obtained  $P'_{\text{app}}/P_{\text{app}}$  by plotting  $c'_{\text{e,app}} \ln \frac{c' - c'_{\text{e,app}}}{c'_1 - c'_{\text{e,app}}}$  versus  
408  $c_{\text{e,app}} \ln \frac{c - c_{\text{e,app}}}{c_1 - c_{\text{e,app}}}$  (Fig. 9), and calculated  $\delta D_{\text{soil,app}}$  by use of Eq. (5). Then we  
409 retrieved  $\delta D_{\text{soil,true}}$  by use of the flask sampling model (Fig. 10d). The  
410 corresponding correction coefficients for  $\delta D_{\text{soil,app}}$  for each net-emission  
411 experiment are shown in Table 3. More information about the retrievals of  
412  $\alpha_{\text{soil,true}}$  and  $\delta D_{\text{soil,true}}$  can be found in Appendix A.

413

414 Overall, the sampling effect on  $\delta D_{\text{soil}}$  is small (less than 22‰). This means that  
415 the flask sampling system strongly affects the temporal evolution of HH and  
416 HD individually (Fig. 5), and the uptake and production rates derived from flask  
417 measurements, but the effects on the computed isotopic signature of the source  
418 and sink are relatively small. More details and discussion of the flask sampling  
419 model corrections are provided in Appendix A.

420

421

### 422 **3. Results**

423

#### 424 **3.1 Temporal evolution of H<sub>2</sub>, HD and $\delta D$**

425

426 Fig. 6 shows examples for the temporal evolution of H<sub>2</sub>, HD and  $\delta D$  in Cabauw  
427 and Speuld, with error estimates included. The errors for H<sub>2</sub> and HD are about 4%  
428 of the respective mole fraction. The error for  $\delta D$  ranges from 2 ‰ to 17 ‰.

429

430 Some of our Cabauw experiments show net soil emission of H<sub>2</sub> (upper panels)  
431 and some show net soil uptake (middle panels), while all Speuld experiments  
432 show net uptake of H<sub>2</sub> (lower panels). In the Cabauw net emission experiments,  
433 the increase in H<sub>2</sub> mole fractions is associated with a strong decrease in  $\delta D$ ,  
434 showing a strongly depleted H<sub>2</sub> source. However, the net uptake experiments at

435 Cabauw show also a decrease in  $\delta D$ , albeit smaller. In the Speuld experiments,  
436 the uptake of  $H_2$  is much faster; the  $\delta D$  increases in the beginning but then  
437 decreases again towards the end of the sampling, when the  $H_2$  mole fractions are  
438 low.

439

440 As mentioned in the introduction, soil uptake tends to increase  $\delta D$  while soil  
441 emission tends to decrease  $\delta D$  of  $H_2$ . The continuous decrease of  $\delta D$  with time  
442 in all Cabauw experiments and the eventual decrease of  $\delta D$  in all Speuld  
443 experiments clearly show that there is concurrent soil emission even with net  
444 uptake. Thus, the equilibrium  $H_2$  concentration in our experiments is not just a  
445 threshold concentration where microbial uptake stops, but the isotopic evolution  
446 shows that there is an active overlapping emission (Conrad, 1994).

447

448

### 449 **3.2 Emission and uptake strength of $H_2$**

450

451 The production rate  $P = P_{\text{true}}$  and uptake rate constant  $k = k_{\text{true}}$  were obtained by  
452 applying exponential fits to the temporal evolution of  $H_2$ , and applying the  
453 corrections derived from the flask sampling model (appendix A) to the  $P_{\text{app}}$  and  
454  $k_{\text{app}}$  obtained from the exponential fits (Fig. 6). The deposition velocity ( $v_d$ ),

455 production flux ( $F_p$ ), initial uptake flux ( $F_u$ ) and net flux at the beginning of the  
456 experiment ( $F_n$ ) were then calculated as follows:

457

$$v_d = kh \quad (7)$$

458

$$F_p = \frac{Ph}{V_M} \quad (8)$$

459

$$F_u = \frac{kc_1h}{V_M} \quad (9)$$

460

$$F_n = F_p - F_u \quad (10)$$

461

462 where  $h$ ,  $V_M$  and  $c_1$  are the chamber height, standard molar volume (=22.4 L  
463 mol<sup>-1</sup>) and H<sub>2</sub> mole fraction of the first flask, respectively. We note that with our  
464 method we derive  $v_d$  as deposition velocity for the gross uptake, unlike most of  
465 the results reported in the literature that just measured net uptake.

466

467 The strongest soil uptake occurs in the Speuld experiments (Table 1a), with a  
468 mean  $v_d$  of (0.17±0.02) (2 SE, n=12) cm s<sup>-1</sup> (SE represents standard error). On  
469 average, the Cabauw experiments show weaker soil uptake, with a mean  $v_d$  of  
470 (0.13±0.06) (2 SE, n=8) cm s<sup>-1</sup> for the net-uptake experiments (Table 1b) and

471 (0.06±0.03) (2 SE, n=9) cm s<sup>-1</sup> for the net-emission experiments (Table 2). In  
472 terms of the net H<sub>2</sub> flux  $F_n$ , this is (-26.5±4.8) (2 SE, n=12) nmol m<sup>-2</sup> s<sup>-1</sup> for  
473 Speuld experiments (Table 1a), (-13.6±8.6) (2 SE, n=8) nmol m<sup>-2</sup> s<sup>-1</sup> for Cabauw  
474 net-uptake experiments (Table 1b) and (49.5±29.8) (2 SE, n=9) nmol m<sup>-2</sup> s<sup>-1</sup> for  
475 Cabauw net-emission experiments (Table 2), indicating strong uptake, weaker  
476 uptake and strong emission of H<sub>2</sub>, respectively.

477

478

### 479 **3.3 Fractionation during soil uptake**

480

481 Soil uptake and soil emission have opposite effects on the isotopic composition  
482 of H<sub>2</sub> and can partly cancel each other. This will lead to additional uncertainty  
483 and we expect to obtain the most robust fractionation factor for soil uptake  
484 when the soil uptake is larger than the soil emission (Table 1a&b).

485

486 The resulting  $\alpha_{\text{soil}}$  for Speuld (Table 1a) varies from 0.913 to 0.955, with a mean  
487 value of 0.937±0.008 (2 SE, n=12). Error estimates for HH and HD mole  
488 fraction at time t and at equilibrium are considered for the final error estimates  
489 of  $\alpha_{\text{soil}}$  for each experiment.

490

Table 1b shows  $\alpha_{\text{soil}}$  of the Cabauw net-uptake experiments. It should be noted that the soil emitted  $\text{H}_2$  interferes much more with the fractionation during uptake in these Cabauw net-uptake experiments than for the Speuld experiments, which is illustrated by the consistent decrease in  $\delta\text{D}$  in the middle panel of Fig. 6. The derived values for  $\alpha_{\text{soil}}$  vary from 0.911 to 1.019 with a mean value of  $0.951 \pm 0.026$  (2 SE,  $n=8$ ) for these 8 selected Cabauw net-uptake experiments. Both the mean and the standard error are higher than for the Speuld experiments ( $0.937 \pm 0.008$ ), but the difference is not significant at the 0.1 confidence level.

To graphically illustrate the calculation of  $\alpha_{\text{soil}}$  with the mass balance model, we plot  $\ln \frac{c' - c'_{\text{e,app}}}{c'_1 - c'_{\text{e,app}}}$  versus  $\ln \frac{c - c_{\text{e,app}}}{c_1 - c_{\text{e,app}}}$  for all Speuld and Cabauw net-uptake experiments in Fig. 7. A linear fit is applied to all the data and the overall  $\alpha_{\text{soil,app}}$  is found to be  $0.947 \pm 0.004$  (95% CI). Applying a correction factor is not straightforward now because this analysis combines the results from different experiments. If we use the average of  $\alpha_{\text{soil,true}} / \alpha_{\text{soil,app}}$  ratios (0.998) for all net-uptake experiments in Table 3 as the correction coefficient for this overall  $\alpha_{\text{soil,app}}$ , the overall  $\alpha_{\text{soil}}$  is  $0.945 \pm 0.004$  (95% CI).

Fig. 8 shows  $\alpha_{\text{soil}}$  as a function of  $v_d$  for all Speuld experiments and Cabauw net-uptake experiments. The  $R^2$  value is nearly zero and the p-value is 0.53 for the linear regression of all experiments, so no significant correlation between  $\alpha_{\text{soil}}$

512 and  $v_d$  is found. Also, no significant correlation is found when considering the  
513 Speuld and Cabauw net-uptake experiments separately.

514

515

### 516 **3.4 Isotopic signature of H<sub>2</sub> emitted from soil**

517

518 As discussed in Section 2.4, the isotopic signature of H<sub>2</sub> emitted from the soil  
519 ( $\delta D_{\text{soil}}$ ) can be obtained from the mass balance model. In order to minimize the  
520 influence of soil uptake on the computed  $\delta D_{\text{soil}}$  and obtain the most robust result,

521 we only consider the Cabauw experiments with strong soil emission and weak  
522 soil uptake ( $c_{e,\text{app}} > 1500$  ppb). In total, 9 Cabauw experiments are selected

523 (Table 2) and a linear fit is applied to the plot of  $c'_{e,\text{app}} \ln \frac{c'_1 - c'_{e,\text{app}}}{c'_1 - c_{e,\text{app}}}$  versus

524  $c_{e,\text{app}} \ln \frac{c - c_{e,\text{app}}}{c_1 - c_{e,\text{app}}}$  for each experiment (Fig. 9). It can be seen that the linear

525 function fits the data very well for each experiment. The slope of the linear fit

526 yields  $P'_{\text{app}}/P_{\text{app}}$ . This  $P'_{\text{app}}/P_{\text{app}}$  ratio is used to calculate  $\delta D_{\text{soil,app}}$  (Eq. (5)). After

527 correcting for the flask sampling effects (see Appendix A), the corresponding

528  $\delta D_{\text{soil}}$  values are shown in Table 2. The  $\delta D_{\text{soil}}$  value ranges from -629 ‰ to -

529 451 ‰, with a mean value of  $(-530 \pm 40)$  ‰ (2 SE, n=9), which is very D-

530 depleted, but still considerably enriched relative to the value around -700 ‰

531 expected for thermodynamic equilibrium between H<sub>2</sub> and H<sub>2</sub>O (Bottinga, 1969).

532

533

## 534 **4. Discussion**

535

### 536 **4.1 Emission and uptake strength of H<sub>2</sub>**

537

538 The deposition velocity  $v_d$  is a measure of the strength of soil uptake. Both  
539 microbial removal and diffusion can affect  $v_d$ , and they can both be influenced  
540 by the temperature and moisture content of the soil (Ehhalt and Rohrer, 2013a;  
541 2013b). On average, the  $v_d$  obtained in this study is larger in the forest region  
542 (Table 1a) than in the grass/clover region (Table 1b and 2), in agreement with  
543 the conclusion from Ehhalt and Rohrer (2009).

544

545 The  $v_d$  of  $(0.06 \pm 0.03)$  cm s<sup>-1</sup> found in our Cabauw net-emission experiments  
546 (Table 2) is similar to those reported in Conrad and Seiler (1980) (0.07 cm s<sup>-1</sup>,  
547 both grass and clover) and Gerst and Quay (2001) (0.04 cm s<sup>-1</sup>, grass), while the  
548  $v_d$  of  $(0.13 \pm 0.06)$  cm s<sup>-1</sup> in Cabauw net-uptake experiments (Table 1b) is larger  
549 than those studies with similar soil cover but close to values of 0.12 to 0.14 cm  
550 s<sup>-1</sup> found in savanna soil (Conrad and Seiler, 1985). The stronger soil uptake in  
551 Speuld forest  $((0.17 \pm 0.02)$  cm s<sup>-1</sup>) agrees well with the beech forest results (0.06  
552 to 0.22 cm s<sup>-1</sup>) in Förstel (1988) and Förstel and Führ (1992). However, other



553 studies at forest sites cited in Ehhalt and Rohrer (2009) showed lower  $v_d$  than  
554 our Speuld results. We note here that the  $v_d$  values reported in Conrad and Seiler  
555 (1980; 1985) were gross deposition velocities while those reported in Gerst and  
556 Quay (2001) were net deposition velocities. The specific method used to obtain  
557  $v_d$  was not documented in the other studies.  $v_d$  obtained from our experiments  
558 are gross deposition velocities.

559

560 The net uptake flux  $F_n$  in our Speuld experiments and Cabauw net-uptake  
561 experiments is much larger than those found in Smith-Downey et al. (2008).  
562 They found a  $F_n$  of about  $-8 \text{ nmol m}^{-2} \text{ s}^{-1}$  for the forest, desert, and marsh, which  
563 was similar to that for loess loamy soil in Schmitt et al. (2009). Our results are  
564 within the  $F_n$  range found in the mixed wood plains by Constant et al. (2008b)  
565 and the Harvard forest by Meredith (2012). Previously at our Cabauw site, Popa  
566 et al. (2011) obtained a  $F_n$  of only  $-3 \text{ nmol m}^{-2} \text{ s}^{-1}$  by using the radon tracer  
567 method. However, the Cabauw net-uptake experiments used for this evaluation  
568 were from selected places where uptake was strong, while the results in Popa et  
569 al. (2011) represented the overall uptake in the footprint of the Cabauw site,  
570 which is a much larger area (tens of  $\text{km}^2$ ).

571

572 Khdhiri et al. (2015) performed microbiological analyses on soil samples from  
573 the Cabauw and Speuld sites, in order to find the drivers of soil  $\text{H}_2$  uptake. They  
574 observed that the  $\text{H}_2$  uptake rate under standard incubation conditions was

575 significantly lower for the Cabauw soil samples than for the Speuld ones, which  
576 is consistent with our findings. The main factors that explained the differences  
577 were the relative abundance of high affinity H<sub>2</sub>-oxydizing bacteria and the soil  
578 carbon content, both lower on average for the Cabauw site.

579

580 The emission of H<sub>2</sub> from the soil is large for the Cabauw net-emission  
581 experiments, with  $F_n$  ranging from 13.7 to 150.2 nmol m<sup>-2</sup> s<sup>-1</sup> and a median  
582 value of 41.0 nmol m<sup>-2</sup> s<sup>-1</sup> (Table 2). One experiment, “CBW-28”, shows  
583 unusually high emission, with H<sub>2</sub> increasing to 3010 ppb within 30 minutes. In  
584 comparison, Conrad and Seiler (1980) found a  $F_n$  of 23-32 nmol m<sup>-2</sup> s<sup>-1</sup> for a  
585 clover field. Except for the experiments “CBW-28” and “CBW-31”, our  
586 Cabauw net-emission experiments are close to the  $F_n$  found by them. The  
587 variability in  $F_n$  could be attributed to different N<sub>2</sub> fixation flux in our  
588 experiments, which could be affected by both spatial density of N<sub>2</sub> fixation  
589 organisms and their N<sub>2</sub> fixation activities. The N<sub>2</sub> fixation activity could be  
590 regulated by various factors including temperature, moisture, light availability  
591 and carbon storage etc. (Belnap, 2001), which were not measured are therefore  
592 not discussed here.

593

594

## 595 **4.2 Fractionation during soil uptake**

596

597 Fractionation during soil uptake of  $H_2$  can happen during the diffusion into the  
598 soil and due to microbial removal within the soil. To further investigate the  
599 factors determining  $\alpha_{\text{soil}}$ , information about the soil cover is provided in Table  
600 1a&b. It is evident that no large differences exist between the Douglas fir,  
601 spruce and beech sites, i.e. the variability between sites is similar to the  
602 variability within sites. The small number of experiments impedes examining  
603 the possible small differences between sites. In order to investigate the diffusion  
604 effect, we removed the soil cover in experiments “SPU-8” and “SPU-12” at the  
605 same place of experiments “SPU-7” and “SPU-11”. The removal of leaves  
606 (“SPU-8”) and needles (“SPU-12”) increased  $\alpha_{\text{soil}}$  by  $\approx 0.014$ , thus towards  
607 smaller fractionation, which indicates that diffusion contributes to the  
608 fractionation. As  $v_d$  also increases when the soil cover is removed, faster  
609 deposition is associated with smaller fractionations in these experiments, which  
610 is similar to the results from Rice et al. (2011).

611

612 The  $\alpha_{\text{soil}}$  for the Cabauw net-uptake experiments is higher and more scattered  
613 than that for the Speuld experiments ( $0.951 \pm 0.026$  vs.  $0.937 \pm 0.008$ ). This could  
614 be caused by the interference of D-depleted  $H_2$  from the strong soil emission in  
615 Cabauw, which may not be perfectly captured via the mathematical models  
616 applied. As can be seen from the strong decline of  $\delta D$  with time in the middle  
617 panel of Fig. 6, though soil uptake of  $H_2$  dominates for the Cabauw net-uptake

618 experiments, soil production is still considerable. If part of the source signature  
619 is not taken into account properly and appears in  $\alpha_{\text{soil}}$ , then  $\alpha_{\text{soil}}$  will be larger,  
620 because soil production tends to decrease  $\delta D$  of  $H_2$ . This could explain why  $\alpha_{\text{soil}}$   
621 is even larger than 1 in “CBW-7”.

622

623 The overall  $\alpha_{\text{soil}}$  (0.945) obtained by plotting  $\ln \frac{c' - c'_{e,\text{app}}}{c'_1 - c'_{e,\text{app}}}$  versus  $\ln \frac{c - c_{e,\text{app}}}{c_1 - c_{e,\text{app}}}$  and  
624 applying the average correction factor for all the Speuld and Cabauw net-uptake  
625 experiments is similar to the results of  $0.943 \pm 0.024$  from Gerst and Quay (2001)  
626 and  $0.94 \pm 0.01$  from Rahn et al. (2002a). They suggested that the overall  $\alpha_{\text{soil}}$  is  
627 more accurate as it is less susceptible to outliers. We argue here that the average  
628  $\alpha_{\text{soil}}$  of all individual experiments in Speuld (0.937) and Cabauw (0.951) is  
629 representative for a spatially averaged fractionation factor for those sites and is  
630 useful for e.g. characterizing the phenomenon and comparing with other  
631 fractionation results. If all experiments are included in one fit, their weight for  
632 determining the slopes depends on how much  $H_2$  has been removed, so  
633 experiments with a lower  $c_{e,\text{app}}$  have a larger weight than experiments with a  
634 higher  $c_{e,\text{app}}$  (i.e. experiments with a higher  $v_d$  have a larger weight than  
635 experiments with a lower  $v_d$ ). The fractionation factor obtained by fitting all  
636 data together is therefore representative for a flux weighted average, which is  
637 the relevant number for the global atmospheric isotope budget.

638

### 639 4.3 Relationship between $\alpha_{\text{soil}}$ and $v_d$

640

641 Rice et al. (2011) proposed a significant positive correlation between  $\alpha$  and  
642 deposition velocity  $v_d$  in their soil uptake experiments. Fig. 8 shows that no  
643 significant correlation between  $\alpha_{\text{soil}}$  and  $v_d$  is found when considering all Speuld  
644 and Cabauw net-uptake experiments. The uptake rate is much stronger in the  
645 Speuld experiments ( $v_d \approx 0.17 \text{ cm s}^{-1}$ ) than in the study of Rice et al. (2011) ( $v_d$   
646  $\approx 0.04 \text{ cm s}^{-1}$ ), but the  $\alpha_{\text{soil}}$  is virtually identical (0.937 *versus* 0.934). Therefore,  
647 when the results from both studies are combined, the correlation reported in  
648 Rice et al. (2011) between  $\alpha_{\text{soil}}$  and  $v_d$  disappears. We suggest that a positive  
649 correlation between  $\alpha_{\text{soil}}$  and  $v_d$  may exist for a specific site where microbial  
650 species are similar. This was suggested from the simultaneous increase of both  
651  $\alpha_{\text{soil}}$  and  $v_d$  in two experiments (“SPU-8” and “SPU-12”), when soil cover was  
652 removed at the same sampling location, as mentioned in Section 4.2.

653

654 We conclude that there is certainly not one single correlation between  $\alpha_{\text{soil}}$  and  
655  $v_d$  that holds globally and the soil type might play an important role.  
656 Measurements at more sites may be needed to positively confirm whether local  
657 positive correlations between  $\alpha_{\text{soil}}$  and  $v_d$  are common.

658

659

#### 660 **4.4 $\delta D$ of $H_2$ emitted from the soil**

661

662 The present study is the first field study to report  $\delta D$  of  $H_2$  emitted from soils.

663 The  $\delta D_{\text{soil}}$  values (-629 ‰ to -451 ‰) shown in Table 2 are less depleted than

664 the  $H_2$  in isotopic equilibrium with water ( $\approx -700$  ‰). Previous observations

665 from environmental  $H_2$  production yielded a  $\delta D$  of -628 ‰ for two seawater

666 samples (Rice et al., 2010), -778 ‰ for a termite headspace sample and -690 ‰

667 for two headspace samples from a eutrophic water pond (Rahn et al., 2002b).

668 Kawagucci et al. (2015) proposed that microbiological  $H_2$  consumption and

669 production could destroy the thermal isotopic equilibrium between  $H_2$  and  $H_2O$

670 in low-temperature hydrothermal fluids. Luo et al. (1991) and Walter et al.

671 (2012) found fractionation factors of 0.448, 0.401 and 0.363 for  $H_2$  generated

672 from water by different  $N_2$ -fixing bacteria in the laboratory.

673

674 In order to compare our  $\delta D_{\text{soil}}$  with the fractionation factors between  $H_2$  and

675  $H_2O$  found by Luo et al. (1991) and Walter et al. (2012), we converted their

676 fractionation factors to  $\delta D(H_2)$  by assuming the  $\delta D(H_2O)$  to be the same as that

677 of global rainwater (-37.8 ‰, Hoffmann et al., 1998). This results in  $\delta D(H_2)$

678 values of -651 ‰ to -569 ‰ for their  $N_2$ -fixing bacteria. Although the ranges

679 are considerable, it appears that the mean  $\delta D_{\text{soil}}$  (-530 ‰) obtained in our field

680 study is even higher than what was found for nitrogenase-derived H<sub>2</sub> in  
681 laboratory experiments.

682

683 It is known that H<sub>2</sub> produced by biogenic N<sub>2</sub> fixation can be largely recycled  
684 within the soil before entering the atmosphere (Evans et al., 1987; Conrad and  
685 Seiler, 1979; 1980). If this uptake process within the soil tends to increase the  
686  $\delta D$  of the remaining H<sub>2</sub>, as the soil uptake process for atmospheric H<sub>2</sub> does, then  
687 the H<sub>2</sub> entering the atmosphere will be less D-depleted than pure biogenic H<sub>2</sub>.  
688 However, if the fractionation factor of removal in the soil is similar to that  
689 determined from the net-uptake experiments ( $\approx 0.94$ ), a large fraction ( $f_{in}$ ) of H<sub>2</sub>  
690 needs to be removed in the soil before release to explain the D-enriched  $\delta D_{soil}$

691 compared to the values reported in the literature. The fraction  $f_{in}$  could in  
692 principle be estimated from the Rayleigh equation:

$$(1 - f_{in})^{\alpha_{in}-1} = \frac{\delta D_{soil} + 1}{\delta D_0 + 1}$$

693 where  $\alpha_{in}$  is the fractionation constant of H<sub>2</sub> within soil,  $\delta D_0$  is the  $\delta D$  value of  
694 initial H<sub>2</sub> produced by N<sub>2</sub>-fixers, and  $\delta D_{soil}$  is the  $\delta D$  value of remaining H<sub>2</sub>  
695 emitted from soil that is measured in our experiments. By assuming  $\alpha_{in}=0.945$   
696 (overall fractionation factor as determined in our deposition experiments),  
697  $\delta D_{soil}=-530\text{‰}$  (averaged  $\delta D_{soil}$  of Cabauw net-emission experiments) and  $\delta D_0=-$   
698  $611\text{‰}$  (averaged of  $\delta D(H_2)$  derived from laboratory experiments in Luo et al.  
699 (1991) and Walter et al. (2012)), we would obtain  $f_{in}=0.97$ . That is, 97% of H<sub>2</sub>

produced by  $N_2$  fixation would be removed within soil before entering atmosphere. This is higher than the estimate from Conrad and Seiler (1979), which was from 30% to 90%. It should be noted that the estimation of  $f_{in}$  is very uncertain due to the lack of information about  $\alpha_{in}$  and  $\delta D_0$ . By using the lower limit of  $\alpha_{in}$  (0.911) in our experiment and the upper limit of  $\delta D_0$  (-569 ‰) in Luo et al. (1991) and Walter et al. (2012), we calculate a lower limit of  $f_{in}$  to be 0.62. The upper limit of  $f_{in}$  is 1.00 when  $\alpha_{in}$  approaches 1. For these calculations we have used a  $\delta D_{soil}$  of -530 ‰, but it varies from -629 ‰ to -451 ‰ in our experiments. We cannot rule out cases with  $\delta D_{soil} = \delta D_0$ , which yields a  $f_{in}$  of 0.

The deuterium enrichment in the emitted  $H_2$ , compared to the value expected in isotopic equilibrium with water, could also be caused by different fractionations induced by different enzymes and/or a potentially enriched deuterium content of the substrate water available for  $H_2$  production in Cabauw.  $H_2$  is generated from the reduction of hydrogen ions ( $H^+$  or  $D^+$ ) in intracellular water (Yang et al., 2012). It was found that the isotopic composition of intracellular water can be different from that of extracellular water due to metabolic processing (Kreuzer-Martin et al., 2006). Due to the differences in H-bonding and hydrogen ion transport, the fractionation may be different for different microbe species, which could result in different isotopic signatures of the produced  $H_2$ . Measurements of the isotopic composition of produced  $H_2$  may be a tool to investigate such effects.



722

723 Finally, we note that if our Cabauw net-emission experiments are analyzed with  
724 a simple Keeling plot approach (i.e. without considering uptake), the y axis  
725 intercept is -703 ‰. We know from the temporal evolution of H<sub>2</sub>, HD and δD  
726 that this model is not adequate and that uptake was significant in our  
727 experiments, so a simple Keeling plot analysis can be misleading if uptake is  
728 not considered.

729

730

## 731 **5. Conclusions**

732

733 This study investigated the isotope effects associated with the production and  
734 uptake of atmospheric H<sub>2</sub> by soil. Our aim was to quantify the fractionation  
735 factor  $\alpha_{\text{soil}}$  for H<sub>2</sub> deposition and the isotopic signature of H<sub>2</sub> emitted from the  
736 soil (δD<sub>soil</sub>) from experiments carried out at Speuld and Cabauw.

737

738 The experiments covered a wide range of conditions from situations with very  
739 strong net H<sub>2</sub> uptake to situations with very strong net H<sub>2</sub> emission. The  
740 superposition of deposition and production made the analysis with simple  
741 models like Rayleigh plot and Keeling plot impossible. Therefore, the mass  
742 balance model suggested by Rice et al. (2011) was used for evaluation.

743

744 The deposition velocity  $v_d$  was largest in the Speuld experiments ( $(0.17 \pm 0.02)$   
745  $\text{cm s}^{-1}$ ) where also the strongest net soil uptake occurred, followed by the  
746 Cabauw net-uptake experiments ( $(0.13 \pm 0.06) \text{ cm s}^{-1}$ ) and Cabauw net-emission  
747 experiments ( $(0.06 \pm 0.03) \text{ cm s}^{-1}$ ). The net  $\text{H}_2$  flux  $F_n$  was  $(-26.5 \pm 4.8) \text{ nmol m}^{-2}$   
748  $\text{s}^{-1}$  for Speuld experiments,  $(-13.6 \pm 8.6) \text{ nmol m}^{-2} \text{ s}^{-1}$  for Cabauw net-uptake  
749 experiments and  $(49.5 \pm 29.8) \text{ nmol m}^{-2} \text{ s}^{-1}$  for Cabauw net-emission  
750 experiments.

751

752 The mean fractionation factors  $\alpha_{\text{soil}}$  are  $0.937 \pm 0.008$  for the Speuld forest soil  
753 experiments and  $0.951 \pm 0.026$  for the Cabauw grassland experiments, which are  
754 representative for a spatial average and useful for comparisons with other  
755 fractionation studies. The Cabauw results may be affected by the relatively  
756 strong concomitant soil emissions. The overall  $\alpha_{\text{soil}}$  by considering all net-  
757 uptake experiments is  $0.945 \pm 0.004$ , which is representative for a flux weighted  
758 average and useful for global isotope budget estimates. The fractionation factors  
759 found in this work are in good agreement with previous studies.

760

761 No significant correlation between  $\alpha_{\text{soil}}$  and deposition velocity  $v_d$  was found  
762 while considering all of our experiments. The  $v_d$  were overall much larger in our  
763 study than those in Rice et al. (2011) and we obtained similar values for  $\alpha_{\text{soil}}$ .  
764 This demonstrates that the positive correlation that was found previously does

765 not hold globally. From two of our Speuld experiments,  $\alpha_{\text{soil}}$  increased after the  
766 removal of leaves or needles above the soil. This indicates that there may be a  
767 fractionation associated with diffusion through the surface layer of leaves or  
768 needles during soil uptake, but more experiments are required to confirm this.

769

770 The isotopic analysis clearly showed that the net uptake was always a  
771 superposition of a larger gross uptake and a gross emission flux. In Cabauw, the  
772 emission strength was very large at locations where clover was present. Using a  
773 simple mass balance approach, the isotopic composition of the emitted  $\text{H}_2$  was  
774 determined to be  $(-530 \pm 40) \text{‰}$ , which is significantly higher than the value  
775 expected for  $\text{H}_2\text{O} - \text{H}_2$  isotope equilibrium. Although limited, other published  
776 data on  $\text{H}_2$  produced biologically via nitrogenase show also a tendency to more  
777 enriched values. An additional isotope enrichment in our field soil study could  
778 originate from fractionation during the recycling of  $\text{H}_2$  within the soil before it  
779 enters the atmosphere.

780

## 781 **Appendix A**

782

### 783 **A1. Flask sampling model**

784

785 A mathematical model is used to simulate the sampling and to correct for the  
786 effects of the flask sampling method on the values of uptake rate constant ( $k$ ),  
787 production rate ( $P$ ), fractionation factor ( $\alpha_{\text{soil}}$ ) and isotopic signature of  $\text{H}_2$   
788 produced from soil ( $\delta\text{D}_{\text{soil}}$ ). We start with a pair of known (*true*) uptake and  
789 production rates and simulate the evolution of the mole fractions of  $\text{H}_2$  and HD  
790 in the flasks and chamber. From the modeled mole fractions we calculate the  
791 *apparent* uptake and production rates and derive the correction needed to obtain  
792 the *true* uptake and production rates from measurement of the *apparent* rates in  
793 actual experiments.

794

#### 795 **A1.1 Mathematical description of the flask sampling model**

796

797 The sampling setup is shown in Fig. 2 of the main paper. After 10 minutes of  
798 flushing, the chamber and the flasks contain ambient air with the prevailing  $\text{H}_2$   
799 and HD mole fractions. In the following we denote  $c_1(t)$ ,  $c_2(t)$ ,  $c_3(t)$ ,  $c_4(t)$  and  
800  $c_0(t)$  the  $\text{H}_2$  mole fractions for the first, second, third, forth flask and the  
801 chamber, respectively. The moment when the first flask and the chamber lid are

802 closed is considered the starting time of the experiment ( $t=0$ ). From this point  
 803 on, only the chamber, the second, third and fourth flask are connected, and the  
 804 initial  $H_2$  mole fraction inside them is  $c_0(0) = c_2(0) = c_3(0) = c_4(0) = c_1$ . We start  
 805 a simulation with an input uptake rate constant ( $k_{\text{true}}$ ) and an input production  
 806 rate ( $P_{\text{true}}$ ). The simulation of the flask sampling is based on Eqs. (A1)-(A4)  
 807 shown below.

808

809 Assuming that the air in each flask and in the chamber is well-mixed during the  
 810 entire sampling process, the time evolution for the second flask  $c_2(t)$ , the third  
 811 flask  $c_3(t)$ , the forth flask  $c_4(t)$  and the chamber  $c_0(t)$  in the first 10 minutes after  
 812 starting the experiment can be expressed as:

813

$$\frac{dc_2(t)}{dt} = \frac{f}{V} c_0(t) - \frac{f}{V} c_2(t) \quad (\text{A1})$$

814

$$\frac{dc_3(t)}{dt} = \frac{f}{V} c_2(t) - \frac{f}{V} c_3(t) \quad (\text{A2})$$

815

$$\frac{dc_4(t)}{dt} = \frac{f}{V} c_3(t) - \frac{f}{V} c_4(t) \quad (\text{A3})$$

816

$$\frac{dc_0(t)}{dt} = \frac{f}{V'} c_4(t) - \frac{f}{V'} c_0(t) + (P_{\text{true}} - k_{\text{true}} c_0(t)) \quad (\text{A4})$$

817

818 where  $V$  and  $V'$  are the air volumes of the flask and chamber, and  $f$  is the flow  
819 rate. These differential equations are solved using the Matlab ODE solvers at  
820 time steps of 0.01 min. The input parameters are  $c_0(0)$ ,  $P_{\text{true}}$ ,  $k_{\text{true}}$ ,  $V$ ,  $V'$  and  $f$ .  
821 For each time step the solvers calculate the hydrogen flux into and out of the  
822 chamber and each flask, as well as the new mole fractions there.

823

824 After 10 minutes, the second flask is closed and now contains air with mole  
825 fraction  $c_2 = c_2(10 \text{ min})$ . From this point on, only the chamber, the third and the  
826 fourth flask are connected, and the time evolution of the mole fractions can be  
827 expressed as:

828

$$\frac{dc_3(t)}{dt} = \frac{f}{V} c_0(t) - \frac{f}{V} c_3(t) \quad (\text{A5})$$

829

$$\frac{dc_4(t)}{dt} = \frac{f}{V} c_3(t) - \frac{f}{V} c_4(t) \quad (\text{A6})$$

830

$$\frac{dc_0(t)}{dt} = \frac{f}{V'} c_4(t) - \frac{f}{V'} c_0(t) + (P_{\text{true}} - k_{\text{true}} c_0(t)) \quad (\text{A7})$$

831

832 After another 10 minutes of sampling, the third flask is closed  $c_3 = c_3(20 \text{ min})$ ,  
833 and only the chamber and the fourth flask are connected. Then, the time  
834 evolution for the fourth flask and the chamber can be expressed as:

835

$$\frac{dc_4(t)}{dt} = \frac{f}{V} c_0(t) - \frac{f}{V} c_4(t) \quad (\text{A8})$$

836

$$\frac{dc_0(t)}{dt} = \frac{f}{V'} c_4(t) - \frac{f}{V'} c_0(t) + (P_{\text{true}} - k_{\text{true}} c_0(t)) \quad (\text{A9})$$

837

838 The  $\text{H}_2$  mole fraction inside the chamber and the fourth flask at time  $t=30$   
 839 minutes is  $c_0(30)$  and  $c_4(30)$ .

840

841 In the end, a set of four flasks with mole fractions  $c_1(0)$ ,  $c_2(10 \text{ min})$ ,  $c_3(20 \text{ min})$   
 842 and  $c_4(30 \text{ min})$  is obtained. By fitting this set of four data points with an  
 843 exponential function  $c = ae^{-k_{\text{app}}t} + c_{\text{e,app}}$  (see Eq. (2) in the main paper), we  
 844 can obtain the *apparent* soil uptake rate constant ( $k_{\text{app}}$ ) and equilibrium  
 845 concentration ( $c_{\text{e,app}}$ ) and further calculate *apparent* production rate  
 846 ( $P_{\text{app}} = k_{\text{app}} c_{\text{e,app}}$ ). These apparent rates  $k_{\text{app}}$  and  $P_{\text{app}}$  are different from the assumed  
 847 *true* rates  $k_{\text{true}}$  and  $P_{\text{true}}$ . The flask sampling model enables us to establish a  
 848 relation between  $k_{\text{app}}$  and  $P_{\text{app}}$  and  $k_{\text{true}}$  and  $P_{\text{true}}$ , so that  $k_{\text{true}}$  and  $P_{\text{true}}$  can be  
 849 derived from  $k_{\text{app}}$  and  $P_{\text{app}}$  in actual experiments, where the true values are  
 850 unknown. To accomplish this, simulations are carried out with a wide range of  
 851 values for  $k_{\text{true}}$  and  $P_{\text{true}}$ , and a corresponding dataset of  $k_{\text{app}}$  and  $P_{\text{app}}$  is generated.

852 Similarly, we use a new set of input uptake rate constant  $k'_{\text{true}}$  and production  
853 rate  $P'_{\text{true}}$  for HD, and generate a corresponding dataset of  $k'_{\text{app}}$  and  $P'_{\text{app}}$ .

854

## 855 **A1.2 The correction coefficients for $k$ and $P$**

856

857 Here we discuss an example of the relationship between  $k_{\text{true}}$  and  $k_{\text{app}}$  for the  
858 setup used in some Cabauw experiments ( $V'=22.8$  L,  $f=2$  L min<sup>-1</sup> and  $\Delta t=10$   
859 min). The pressure inside the flasks is 200 kPa and the pressure inside the  
860 chamber is 100 kPa. The relationship between  $k_{\text{true}}/k_{\text{app}}$  and  $k_{\text{app}}$  is shown in Fig.  
861 10a. The ratio  $k_{\text{true}}/k_{\text{app}}$  varies between 1.45 to 1.61 for our  $k_{\text{app}}$  range of 0.04 to  
862 0.30 min<sup>-1</sup>. This relationship does not depend on  $P_{\text{true}}$  (with  $P_{\text{true}}$  varying from 50  
863 to 650 ppb min<sup>-1</sup>). An additional uncertainty can arise from incorrect timing of  
864 the flask sampling, but sampling times should be correct within few seconds,  
865 which may lead to an additional uncertainty of below 1%. The uncertainty of  
866 the flow rate obtained from the rotameter due to variations in ambient pressure  
867 and temperature that were not recorded is less than 4%, and the effect on the  
868 ratio  $k_{\text{true}}/k_{\text{app}}$  ratio is below 1%. We can retrieve  $k_{\text{true}}$  by multiplying  $k_{\text{app}}$  with the  
869 modeled value of  $k_{\text{true}}/k_{\text{app}}$  for each experiment. The ratio  $k_{\text{true}}/k_{\text{app}}$  for each  
870 experiment is shown in Table 3. It depends on experimental setup and  $k_{\text{app}}$  of  
871 each experiment, with a range of 1.177 to 1.589.

872



873 After retrieving  $k_{\text{true}}$  from  $k_{\text{app}}$ , we investigate the relationship between  $P_{\text{true}}/P_{\text{app}}$   
874 and  $P_{\text{app}}$  for a fixed value of  $k_{\text{true}}$  (Fig. 10b). The ratio  $P_{\text{true}}/P_{\text{app}}$  depends slightly  
875 on  $P_{\text{app}}$  and  $k_{\text{true}}$ , ranging from 1.40 to 1.59 for a wide  $P_{\text{app}}$  range of 30 to 450  
876 ppb min<sup>-1</sup> and a wide  $k_{\text{true}}$  range of 0.05 to 0.45 min<sup>-1</sup>. As for the correction of  $k$ ,  
877 uncertainties arising from incorrect timing of the flask sampling and from  
878 pressure and temperature variations and their effect on the flow rate lead to  
879 additional uncertainties of  $P_{\text{true}}/P_{\text{app}}$  ratio below 1%, which are not considered.  
880 We can retrieve  $P_{\text{true}}$  by multiplying  $P_{\text{app}}$  with  $P_{\text{true}}/P_{\text{app}}$  for each experiment after  
881 having determined  $k_{\text{true}}$  from  $k_{\text{app}}$ . The ratio  $P_{\text{true}}/P_{\text{app}}$  for each experiment is  
882 shown in Table 3 and depends on the experimental setup,  $P_{\text{app}}$  and  $k_{\text{app}}$  of each  
883 experiment. It ranges from 1.152 to 2.759 for most experiments, with an  
884 exception of 7.472 for experiment SPU-2 where a very small  $P_{\text{app}}$  of 0.67 ppb  
885 min<sup>-1</sup> is found. Although the ratio  $P_{\text{true}}/P_{\text{app}}$  of experiment SPU-2 is high,  $P_{\text{true}}$  of  
886 SPU-2 is still smaller than the rest of the experiments.  $P_{\text{true}}/P_{\text{app}}$  ratios for  
887 experiments SPU-10 and SPU-11 are null because these two experiments show  
888 a  $P_{\text{app}}$  of zero.

889

### 890 **A1.3 The correction coefficients for $\alpha_{\text{soil}}$ and $\delta D_{\text{soil}}$**

891

892 In our experiments, the uncertainties of  $k_{\text{app}}$  and  $k'_{\text{app}}$  derived from exponential  
893 fits to the time evolution of HH and HD are rather large, which results in a large  
894 scatter of  $\alpha_{\text{soil,app}}$  if  $\alpha_{\text{soil,app}}$  is calculated directly as  $k'_{\text{app}}/k_{\text{app}}$ . Thus, we obtained

895  $\alpha_{\text{soil,app}}$  by plotting  $\ln \frac{c'_1 - c'_{e,\text{app}}}{c'_1 - c'_{e,\text{app}}}$  versus  $\ln \frac{c - c_{e,\text{app}}}{c_1 - c_{e,\text{app}}}$  (Fig. 7) for each experiment

896 which yields a smaller scatter for  $\alpha_{\text{soil,app}}$ .

897

898 Correction coefficients to convert  $\alpha_{\text{soil,app}}$  to  $\alpha_{\text{soil,true}}$  are obtained using the flask

899 sampling model by comparing  $\alpha_{\text{soil,true}}$  used as input for the model run to  $\alpha_{\text{soil,app}}$

900 derived from the plot of  $\ln \frac{c'_1 - c'_{e,\text{app}}}{c'_1 - c'_{e,\text{app}}}$  versus  $\ln \frac{c - c_{e,\text{app}}}{c_1 - c_{e,\text{app}}}$  of the output values, like

901 in the experiments. Fig. 10c shows  $\alpha_{\text{soil,true}}/\alpha_{\text{soil,app}}$  as a function of  $\alpha_{\text{soil,app}}$  for a

902 wide  $\delta D_{\text{soil,true}}$  range of -750‰ to -250‰ with the sampling setup described

903 above ( $V=22.8$  L,  $f=2$  L min<sup>-1</sup> and  $\Delta t=10$  min) for  $k_{\text{true}}=0.25$  min<sup>-1</sup> and  $P_{\text{true}}=50$

904 ppb min<sup>-1</sup>. In this case the correction factor  $\alpha_{\text{soil,true}}/\alpha_{\text{soil,app}}$  varies from 0.98 to

905 1.00 for a  $\alpha_{\text{soil,app}}$  range of 0.90 to 1.00, and it does not depend on  $\delta D_{\text{soil,true}}$ . Thus,

906 after retrieving  $k_{\text{true}}$  and  $P_{\text{true}}$  as described in Section A1.2, we can retrieve  $\alpha_{\text{soil,true}}$

907 from  $\alpha_{\text{soil,app}}$  for each experiment. The correction factors range from 0.984 to

908 1.007, depending on the experimental setup and  $\alpha_{\text{soil,app}}$  of each experiment

909 (Table 3).

910

911 Similarly, in our experiments, the uncertainties of  $P_{\text{app}}$  and  $P'_{\text{app}}$  derived from

912 exponential fits of time evolution of HH and HD are large, which results in a

913 large scatter of  $\delta D_{\text{soil,app}}$  if  $\delta D_{\text{soil,app}}$  is calculated directly from these  $P'_{\text{app}}$  and  $P_{\text{app}}$ .

914 We therefore obtained the ratio  $P'_{\text{app}}/P_{\text{app}}$  by plotting  $c'_{e,\text{app}} \ln \frac{c'_1 - c'_{e,\text{app}}}{c'_1 - c'_{e,\text{app}}}$  versus

915  $c_{e,app} \ln \frac{c - c_{e,app}}{c_1 - c_{e,app}}$  (Fig. 9) and calculated  $\delta D_{soil,app}$  from Eq. (4). This yielded  
 916 smaller scatter for  $\delta D_{soil,app}$ . After retrieving  $k_{true}$ ,  $P_{true}$  and  $\alpha_{soil,true}$  as described  
 917 above, we used the flask sampling model again to derived correction factors by  
 918 comparing  $\delta D_{soil,true}$  used as model input with  $\delta D_{soil,app}$  obtained from  
 919  $c'_{e,app} \ln \frac{c' - c'_{e,app}}{c'_1 - c'_{e,app}}$  versus  $c_{e,app} \ln \frac{c - c_{e,app}}{c_1 - c_{e,app}}$  of the model output, and retrieve  
 920  $\delta D_{soil,true}$  from  $\delta D_{soil,app}$  for each experiment. Fig. 10d shows  
 921  $(\delta D_{soil,true} + 1)/(\delta D_{soil,app} + 1)$  as a function of  $(\delta D_{soil,app} + 1)$  for a  $\alpha_{soil,true}$  range of 0.90  
 922 to 1.00 with the sampling setup described above ( $V'=22.8$  L,  $f=2$  L min<sup>-1</sup> and  
 923  $\Delta t=10$  min) for  $k_{true}=0.25$  min<sup>-1</sup> and  $P_{true}=50$  ppb min<sup>-1</sup>. The ratio  
 924  $(\delta D_{soil,true} + 1)/(\delta D_{soil,app} + 1)$  changes from 0.99 to 1.05 for a wide  $(\delta D_{soil,app} + 1)$   
 925 range of 0.25 to 0.65. It can be seen that the  $(\delta D_{soil,true} + 1)/(\delta D_{soil,app} + 1)$  ratio  
 926 depends slightly on  $\alpha_{soil,true}$  at a fixed  $(\delta D_{soil,app} + 1)$ , with a maximum difference  
 927 of about 1% for a  $\alpha_{soil,true}$  range of 0.90 to 1.00. The ratio  
 928  $(\delta D_{soil,true} + 1)/(\delta D_{soil,app} + 1)$  for each net-emission experiment is shown in Table 3,  
 929 ranging from 1.007 to 1.048. The largest difference between  $\delta D_{soil,true}$  and  
 930  $\delta D_{soil,app}$  is 21‰ for CBW-8. The mean  $\delta D_{true}$  and  $\delta D_{app}$  for these net emission  
 931 experiments are -530‰ and -538‰, respectively.

932

933 In conclusion, the effect of the flask sampling process is relatively small for  $\alpha_{soil}$   
 934 and  $\delta D_{soil}$ , but considerable for the uptake rate constants  $k$  and  $k'$  and emission  
 935 rates  $P$  and  $P'$ . The flask sampling model allows to derive corresponding

936 corrections that have been applied to correct for the bias introduced by the flask  
937 sampling system.

938

939

## 940 **Acknowledgements**

941

942 We are grateful to C. Van der Veen, M. Bolder and H. Snellen for their help on  
943 maintaining the GC-IRMS system and set-up of the sampling. We are also  
944 grateful to Jan Kaiser for giving valuable comments on the flask sampling  
945 model. This work was supported by the Dutch National Science foundation  
946 NWO as part of the NWO-ACTS Sustainable Hydrogen (H<sub>2</sub>) project  
947 2007/00566/ACTS, grant numbers 053.61.026 and 053.61.126.

948

949

950

951

952

953

954

955

956

957

## 958 **References**

959

960 Batenburg, A. M., Walter, S., Pieterse, G., Levin, I., Schmidt, M., Jordan, A.,  
961 Hammer, S., Yver, C., and Röckmann, T.: Temporal and spatial variability of the  
962 stable isotopic composition of atmospheric molecular hydrogen: observations at six  
963 EUROHYDROS stations, *Atmos. Chem. Phys.*, 11, 6985–6999, doi:10.5194/acp-11-  
964 6985-2011, 2011.

965

966 Beljaars, A. C. M. and Bosveld, F. C.: Cabauw data for the validation of land surface  
967 parameterization schemes, *J. Climate*, 10, 1172-1193, doi: 10.1175/1520-  
968 0442(1997)010<1172:CDFTVO>2.0.CO;2, 1997.

969

970 Belnap, J.: Factors influencing nitrogen fixation and nitrogen release in biological soil  
971 crusts, Springer-Verlag, Berlin Heidelberg, 241–261, 2001.

972

973 Bottinga, Y.: Calculated fractionation factors for carbon and hydrogen isotope  
974 exchange in the system calcite-carbon dioxide-graphite-methane-hydrogen-water  
975 vapour, *Geochim. Cosmochim. Ac.*, 33, 49–64, doi:10.1016/0016-7037(69)90092-1,  
976 1969.

977

978 Conrad, R.: Compensation concentration as critical variable for regulating the flux of  
979 trace gases between soil and atmosphere, *Biogeochemistry*, 27, 155–170,  
980 doi:10.1007/BF00000582, 1994.

981

982 Conrad, R. and Seiler W.: Field measurements of hydrogen evolution by nitrogen-  
983 fixing legumes, *Soil Biol. Biochem.*, 11, 689-690, doi: 10.1016/0038-0717(79)90041-  
984 5, 1979.

985

986 Conrad, R. and Seiler, W.: Contribution of hydrogen production by biological  
987 nitrogen fixation to the global hydrogen budget, *J. Geophys. Res.*, 85, 5493-5498, doi:  
988 10.1029/JC085iC10p05493, 1980.

989

990 Conrad, R. and Seiler, W.: Decomposition Of atmospheric hydrogen by soil  
991 microorganisms and soil enzymes, *Soil Biol. Biochem.*, 13, 43–49, doi: 10.1016/0038-  
992 0717(81)90101-2, 1981.

993

994 Conrad, R. and Seiler, W.: Influence of temperature, moisture, and organic carbon on  
995 the flux of H<sub>2</sub> and CO between soil and atmosphere: field studies in subtropical  
996 regions, *J. Geophys. Res.*, 90, 5699–5709, doi: 10.1029/JD090iD03p05699, 1985.

997

998 Conrad, R., Weber, M., and Seiler, W.: Kinetics and electron transport of soil  
999 hydrogenases catalyzing the oxidation of atmospheric hydrogen, *Soil Biol. and*  
1000 *Biochem.*, 15, 167-173, doi: 10.1016/0038-0717(83)90098-6, 1983.

1001

1002 Constant, P., Poissant, L., and Villemur, R.: Isolation of *Streptomyces* sp. PCB7, the  
1003 first microorganism demonstrating high-affinity uptake of tropospheric H<sub>2</sub>, ISME J., 2,  
1004 1066-1076, doi: 10.1038/ismej.2008.59, 2008a.

1005

1006 Constant, P., Poissant, L., and Villemur, R.: Annual hydrogen, carbon monoxide and  
1007 carbon dioxide concentrations and surface to air exchanges in a rural area (Québec,  
1008 Canada), Atmos. Environ., 42, 5090-5100, doi: 10.1016/j.atmosenv.2008.02.021,  
1009 2008b.

1010

1011 Constant, P., Chowdhury, S. P., Pratscher, J., and Conrad, R.: Streptomycetes  
1012 contributing to atmospheric molecular hydrogen soil uptake are widespread and  
1013 encode a putative high-affinity [NiFe]-hydrogenase, Environ. Microbiol., 12, 821-829,  
1014 doi:10.1111/j.1462-2920.2009.02130.x, 2010.

1015

1016 Constant, P., Chowdhury, S. P., Hesse, L., and Conrad, R.: Co-localization of  
1017 atmospheric H<sub>2</sub> oxidation activity and high affinity H<sub>2</sub>-oxidizing bacteria in non-  
1018 axenic soil and sterile soil amended with *Streptomyces* sp. PCB7. Soil Biol.  
1019 Biochem., 43, 1888-1893, doi: 10.1016/j.soilbio.2011.05.009, 2011.

1020

1021 De Wit, J. C., Van der Straten, C. M., and Mook, W. G.: Determination of the  
1022 absolute isotopic ratio of V-SMOW and SLAP, Geostandards Newsletter, 4, 33–36,  
1023 doi:10.1111/j.1751- 908X.1980.tb00270.x, 1980.

1024

1025 Ehhalt, D. H. and Rohrer, F.: The tropospheric cycle of H<sub>2</sub>: a critical review, *Tellus B*,  
 1026 61(3), 500–535, doi:10.1111/j.1600-0889.2009.00416.x, 2009.  
 1027  
 1028 Ehhalt, D. H. and Rohrer, F.: The dependence of soil H<sub>2</sub> uptake on temperature and  
 1029 moisture: a reanalysis of laboratory data, *Tellus B*, 63(5), 1040-1051,  
 1030 doi: 10.1111/j.1600-0889.2011.00581.x, 2011.  
 1031  
 1032 Ehhalt, D. H. and Rohrer, F.: Deposition velocity of H<sub>2</sub>: a new algorithm for its  
 1033 dependence on soil moisture and temperature, *Tellus B*, 65, 19904  
 1034 doi:10.3402/tellusb.v65i0.19904, 2013a.  
 1035  
 1036 Ehhalt, D. H. and Rohrer, F.: Dry deposition of molecular hydrogen in the presence of  
 1037 H<sub>2</sub> production, *Tellus B*, 65, 20620, doi:10.3402/tellusb.v65i0.20620, 2013b.  
 1038  
 1039 Evans, H. J., Harker, A. R., Papen, H., Russell, S. A., Hanus, F. J., and Zuber, M.:  
 1040 Physiology, biochemistry, and genetics of the uptake hydrogenase in rhizobia, *Annu.*  
 1041 *Rev. Microbiol.*, 41(1), 335-361, 1987.  
 1042  
 1043 Gerst, S. and Quay, P.: The deuterium content of atmospheric molecular hydrogen:  
 1044 Method and initial measurements, *J. Geophys. Res.*, 105, 26433–26445,  
 1045 doi:10.1029/2000JD900387, 2000.  
 1046



1047 Förstel, H.: HT to HTO conversion in the soil and subsequent tritium pathway: field  
 1048 release data and laboratory experiments, *Fusion Tech.*, **14**, 1241–1246, 1988.  
 1049  
 1050 Förstel, H. and Führ, F.: Trockene Deposition von Tritium in den Boden, Annual  
 1051 Report, Forschungszentrum Jülich, Jülich, 45–51, 1992.  
 1052  
 1053 Gerst, S. and Quay, P.: Deuterium component of the global molecular hydrogen cycle,  
 1054 *J. Geophys. Res.*, 106, 5021–5031, doi:10.1029/2000JD900593, 2001.  
 1055  
 1056 Gonfiantini, R., Stichler, W., and Rozanski, K.: Standards and intercomparison  
 1057 materials distributed by the International Atomic Energy Agency for stable isotope  
 1058 measurements, in: Reference and intercomparison materials for stable isotopes of light  
 1059 elements: Proceedings of a consultants meeting held in Vienna, 1-3 December 1993,  
 1060 IAEA-TECDOC-825, International Atomic Energy Agency, Vienna, 1993.  
 1061  
 1062 Guo, R. and Conrad, R.: Extraction and characterization of soil hydrogenases  
 1063 oxidizing atmospheric hydrogen, *Soil Biol. Biochem.*, 40(5), 1149–1154,  
 1064 doi:10.1016/j.soilbio.2007.12.007, 2008.  
 1065  
 1066 Häring, V., Klüber, H. D., and Conrad, R.: Localization of atmospheric H<sub>2</sub>-oxidizing  
 1067 soil hydrogenases in different particle fractions of soil, *Biol. Fert. Soils*, 18(2), 109-  
 1068 114, doi:10.1007/BF00336455, 1994.  
 1069

1070 Haumann, F. A., Batenburg, A. M., Pieterse, G., Gerbig, C., Krol, M. C., and  
 1071 Röckmann, T.: Emission ratio and isotopic signatures of molecular hydrogen  
 1072 emissions from tropical biomass burning, *Atmos. Chem. Phys.*, 13, 9401–9413,  
 1073 doi:10.5194/acp-13-9401-2013, 2013.  
 1074  
 1075 Heij, G. H. and Erisman, J. W.: Acid Atmospheric Deposition and Its Effects on  
 1076 Terrestrial Ecosystems in The Netherlands, *Studies in Environmental Sciences* 69,  
 1077 ISBN 0-444-82037-X, Elsevier, Amsterdam, 1997.  
 1078  
 1079 Hoffmann, G., Werner, M., and Heimann, M.: The water isotope module of the  
 1080 ECHAM atmospheric general circulation model – A study on time scales from days to  
 1081 several years, *J. Geophys. Res.*, 103, 16871–16896, doi:10.1029/98JD00423, 1998.  
 1082  
 1083 Jordan, A. and Steinberg, B.: Calibration of atmospheric hydrogen measurements,  
 1084 *Atmos. Meas. Tech.*, 4, 509–521, doi:10.5194/amt-4-509-2011, 2011.  
 1085  
 1086 Kawagucci, S., Toki, T., Ishibashi, J., Takai, K., Ito, M., Oomori, T., and Gamo, T.,  
 1087 Isotopic variation of molecular hydrogen in 20°–375°C hydrothermal fluids as  
 1088 detected by a new analytical method, *J. Geophys. Res.*, 115, G03021,  
 1089 doi:10.1029/2009JG001203, 2010.  
 1090  
 1091 Khdhiri, M., Hesse, L., Popa, M. E., Quiza, L., Lalonde, I., Meredith, L. K.,  
 1092 Röckmann, T., and Constant, P.: Soil carbon content and relative abundance of high

1093 affinity H<sub>2</sub>-oxidizing bacteria predict atmospheric H<sub>2</sub> soil uptake activity better than  
 1094 soil microbial community composition, *Soil Biol. Biochem.*, 85, 1-9,  
 1095 doi:10.1016/j.soilbio.2015.02.030, 2015.  
 1096  
 1097 Kreuzer-Martin, H. W., Lott, M. J., Ehleringer, J. R., and Hegg, E. L.: Metabolic  
 1098 processes account for the majority of the intracellular water in log-phase *Escherichia*  
 1099 *coli* cells as revealed by hydrogen isotopes, *Biochemistry*, 45(45), 13622-13630,  
 1100 doi:10.1021/bi0609164, 2006.  
 1101  
 1102 Luo, Y., Sternberg, L., Suda, S., Kmazawa, S., and Mitsui, A.: Extremely low D/H  
 1103 ratios of photoproduced hydrogen by cyanobacteria, *Plant Cell Physiol.*, 32(6), 897–  
 1104 900, 1991.  
 1105  
 1106 Meredith, L.K.: Field measurement of the fate of atmospheric H<sub>2</sub> in a Forest  
 1107 environment: from canopy to soil, Ph.D. thesis, Department of Earth, Atmospheric  
 1108 and Planetary Sciences, Massachusetts Institute of Technology, United States, 250 pp,  
 1109 2012.  
 1110  
 1111 Novelli, P. C., Lang, P. M., Masarie, K. A., Hurst, D. F., Myers, R., and Elkins, J. W.:  
 1112 Molecular hydrogen in the troposphere: Global distribution and budget, *J. Geophys.*  
 1113 *Res.*, 104, 30427– 30444, doi:10.1029/1999JD900788, 1999.  
 1114

1115 Pieterse, G., Krol, M. C., Batenburg, A. M., Steele, L. P., Krummel, P. B.,  
 1116 Langenfelds, R. L., and Röckmann, T.: Global modelling of H<sub>2</sub> mixing ratios and  
 1117 isotopic compositions with the TM5 model, *Atmos. Chem. Phys.*, 11, 7001–7026,  
 1118 doi:10.5194/acp-11-7001-2011, 2011.  
 1119  
 1120 Pieterse, G., Krol, M. C., Batenburg, A. M., Brenninkmeijer, C. A. M., Popa, M. E.,  
 1121 O’Doherty, S., Grant, A., Steele, L. P., Krummel, P. B., Langenfelds, R. L., Wang, H.  
 1122 J., Vermeulen, A. T., Schmidt, M., Yver, C., Jordan, A., Engel, A., Fisheraffilmark, R.  
 1123 E., Lowry, D., Nisbet, E. G., Reimann, S., Vollmer, M. K., Steinbacher, M., Hammer,  
 1124 S., Forster, G., Sturges, W. T., and Röckmann, T.: Reassessing the variability in  
 1125 atmospheric H<sub>2</sub> using the two-way nested TM5 model, *J. Geophys. Res.-Atmos.*, 118,  
 1126 3764–3780, doi:10.1002/jgrd.50204, 2013.  
 1127  
 1128 Popa, M. E., Vermeulen, A. T., van den Bulk, W. C. M., Jongejan, P. A. C.,  
 1129 Batenburg, A. M., Zahorowski, W., and Röckmann, T.: H<sub>2</sub> vertical profiles in the  
 1130 continental boundary layer: measurements at the Cabauw tall tower in the Netherlands,  
 1131 *Atmos. Chem. Phys.*, 11, 6425–6443, doi:10.5194/acp-11-6425-2011, 2011.  
 1132  
 1133 Price, H., Jaeglé, L., Rice, A., Quay, P., Novelli, P. C., and Gammon, R.: Global  
 1134 budget of molecular hydrogen and its deuterium content: Constraints from ground  
 1135 station, cruise, and aircraft observations, *J. Geophys. Res. -Atmos.*, 112, D22108,  
 1136 doi:10.1029/2006JD008152, 2007.  
 1137

1138 Rahn, T., Eiler, J. M., Kitchen, N., Fessenden, J. E., and Randerson, J. T.:  
 1139 Concentration and  $\delta D$  of molecular hydrogen in boreal forests: Ecosystem-scale  
 1140 systematics of atmospheric  $H_2$ , *Geophys. Res. Lett.*, 29(18), 35-1-35-4,  
 1141 doi:10.1029/2002GL015118, 2002a.  
 1142  
 1143 Rahn, T., Kitchen, N., and Eiler, J.: D/H ratios of atmospheric  $H_2$  in urban air: results  
 1144 using new methods for analysis of nano-molar  $H_2$  samples, *Geochim. Cosmochim.*  
 1145 *Ac.*, 66(14), 2475– 2481, doi:10.1016/S0016-7037(02)00858-X, 2002b.  
 1146  
 1147 Rahn, T., Eiler, J. M., Boering, K. A., Wennberg, P. O., McCarthy, M. C., Tyler, S.,  
 1148 Schauffler, S., Donnelly, S., and Atlas, E.: Extreme deuterium enrichment in  
 1149 stratospheric hydrogen and the global atmospheric budget of  $H_2$ , *Nature*, 424, 918–  
 1150 921, doi:10.1038/nature01917, 2003.  
 1151  
 1152 Rahn, T., Randerson, J. T., and Eiler, J.: Variability of Deuterium Fractionation  
 1153 Associated With Soil Uptake of Atmospheric Molecular Hydrogen, *Eos Trans. AGU*,  
 1154 86(52), Fall Meet. Suppl., Abstract B11A-1031, 2005  
 1155  
 1156 Rhee, T. S., Mak, J., Röckmann, T., and Brenninkmeijer, C. A. M.: Continuous-flow  
 1157 isotope analysis of the deuterium/hydrogen ratio in atmospheric hydrogen, *Rapid*  
 1158 *Commun. Mass Spectrom.*, 18(3), 299–306, doi:10.1002/rcm.1309, 2004.  
 1159

1160 Rice, A., Quay, P., Stutsman, J., Gammon, R., Price, H., and Jaeglé, L.: Meridional  
 1161 distribution of molecular hydrogen and its deu- terium content in the atmosphere, J.  
 1162 Geophys. Res., 115(D12), 1–12, doi:10.1029/2009JD012529, 2010.  
 1163  
 1164 Rice, A., Dayalu, A., Quay, P., and Gammon, R.: Isotopic fractionation during soil  
 1165 uptake of atmospheric hydrogen, Biogeosciences, 8, 763–769, doi:10.5194/bg-8-763-  
 1166 2011, 2011.  
 1167  
 1168 Röckmann, T., Rhee, T. S., and Engel, A.: Heavy hydrogen in the stratosphere, Atmos.  
 1169 Chem. Phys., 3, 2015–2023, doi:10.5194/acpd-3-3745-2003, 2003a.  
 1170  
 1171 Röckmann, T., Kaiser, J., Brenninkmeijer, C. A. M., and Brand, W. A.: Gas  
 1172 chromatography/isotope-ratio mass spectrometry method for high-precision position-  
 1173 dependent  $^{15}\text{N}$  and  $^{18}\text{O}$  measurements of atmospheric nitrous oxide, Rap. Commun.  
 1174 Mass Spectrom., 17, 1897–1908, 2003b.  
 1175  
 1176 Röckmann, T., Álvarez, C. X. G., Walter, S., Veen, C. van der, Wollny, A. G., Gunthe,  
 1177 S. S., Helas, G., Pöschl, U., Keppler, F., Greule, M., and Brand, W. A.: Isotopic  
 1178 composition of  $\text{H}_2$  from wood burning: Dependency on combustion efficiency,  
 1179 moisture content, and  $\delta\text{D}$  of local precipitation, J. Geophys. Res., 115, D17308,  
 1180 doi:10.1029/2009JD013188, 2010.  
 1181

1182 Rothe, M., Jordan, A., and Brand, W. A.: Trace gases,  $\delta^{13}\text{C}$  and  $\delta^{18}\text{O}$  of  $\text{CO}_2$ -in-air  
 1183 samples: Storage in glass flasks using PCTFE seals and other effects, in: GAW report  
 1184 161, 12th WMO/IAEA meeting of experts on carbon dioxide concentration and related  
 1185 tracers measurements techniques, edited by: Worthy, D. and Huang, L., Toronto,  
 1186 Canada, 15–18 September 2003, WMO TD No. 1275, 2004.  
 1187  
 1188 Ruijven, B. van, Lamarque, J. F., Vuuren, D. P. van, Kram, T., and Eerens, H.:  
 1189 Emission scenarios for a global hydrogen economy and the consequences for global  
 1190 air pollution, *Global Environ. Chang.*, 21(3), 983–994, 2011.  
 1191  
 1192 Schmitt, S., Hanselmann, A., Wollschläger, U., Hammer, S., and Levin, I.:  
 1193 Investigation of parameters controlling the soil sink of atmospheric molecular  
 1194 hydrogen. *Tellus B*, 61(2), 416–423, 2009.  
 1195  
 1196 Schultz, M. G., Diehl, T., Brasseur, G. P., and Zittel, W.: Air pollution and climate-  
 1197 forcing impacts of a global hydrogen economy, *Science*, 302(5645), 624–627,  
 1198 doi:10.1126/science.1089527, 2003.  
 1199  
 1200 Smith-Downey, N. V., Randerson, J. T. and Eiler, J. M.: Temperature and moisture  
 1201 dependence of soil  $\text{H}_2$  uptake measured in the laboratory. *Geophys. Res. Lett.*, 33,  
 1202 L14813, doi:10.1029/2006GL026749, 2006.  
 1203

1204 Smith-Downey, N. V., Randerson, J. T., and Eiler, J. M.: Molecular hydrogen uptake  
 1205 by soils in forest, desert, and marsh ecosystems in California, *J. Geophys. Res.-*  
 1206 *Biogeosci.*, 113, G03037, doi:10.1029/2008JG000701, 2008.  
 1207  
 1208 Tromp, T. K., Shia, R. L., Allen, M., Eiler, J. M., and Yung, Y. L.: Potential  
 1209 environmental impact of a hydrogen economy on the stratosphere, *Science*, 300,  
 1210 1740–1742, doi:10.1126/science.1085169, 2003.  
 1211  
 1212 Vogel, B., Feck, T., Grooß, J. U., and Riese, M.: Impact of a possible future global  
 1213 hydrogen economy on Arctic stratospheric ozone loss, *Energy Environ. Sci.*, 5, 6445-  
 1214 6452, doi:10.1039/c2ee03181g, 2012.  
 1215  
 1216 Vollmer, M. K., Walter, S., Mohn, J., Steinbacher, M., Bond, S. W., Röckmann, T.,  
 1217 and Reimann, S.: Molecular hydrogen (H<sub>2</sub>) combustion emissions and their isotope  
 1218 (D/H) signatures from domestic heaters, diesel vehicle engines, waste incinerator  
 1219 plants, and biomass burning, *Atmos. Chem. Phys.*, 12, 6275–6289, doi:10.5194/acp-  
 1220 12-6275-2012, 2012.  
 1221  
 1222 Walter, S., Laukenmann, S., Stams, A. J. M., Vollmer, M. K., Gleixner, G., and  
 1223 Röckmann, T.: The stable isotopic signature of biologically produced molecular  
 1224 hydrogen (H<sub>2</sub>). *Biogeosciences*, 9(10), 4115-4123, 2012.  
 1225



1226 Warwick, N. J., Bekki, S., Nisbet, E. G., and Pyle, J. A.: Impact of a hydrogen  
1227 economy on the stratosphere and troposphere studied in a 2-D model, *Geophys. Res.*  
1228 *Lett.*, 31(5), 2–5, doi:10.1029/2003GL019224, 2004.

1229

1230 Xiao, X., Prinn, R. G., Simmonds, P. G., Steele, L. P., Novelli, P. C., Huang, J.,  
1231 Langenfelds, R. L., O'Doherty, S., Krummel, P. B., Fraser, P. J., Porter, L. W., Weiss,  
1232 R. F., Salameh, P., and Wange, R. H. J.: Optimal estimation of the soil uptake rate of  
1233 molecular hydrogen from the Advanced Global Atmospheric Gases Experiment and  
1234 other measurements, *J. Geophys. Res.*, 112, D07303, doi:10.1029/2006JD007241,  
1235 2007.

1236

1237 Yang, H., Gandhi, H., Shi, L., Kreuzer, H. W., Ostrom, N. E., and Hegg, E. L.: Using  
1238 gas chromatography/isotope ratio mass spectrometry to determine the fractionation  
1239 factor for H<sub>2</sub> production by hydrogenases. *Rapid Commun. Mass Spectrom.*, 26(1),  
1240 61-68, doi: 10.1002/rcm.5298, 2012.

1241

1242

1243

1244

1245

## 1246 Tables

1247

1248 Table 1. The deposition velocity ( $v_d$ ), fractionation factor ( $\alpha_{\text{soil}}$ ) as well as its error estimate,  
 1249 and soil cover information for each Speuld experiment (a) and Cabauw net-uptake  
 1250 experiment (b). The STDEV represents standard deviation and SE represents standard error.  
 1251 The errors of  $\alpha_{\text{soil}}$  represent the 95% confidence interval (CI) for  $\alpha_{\text{soil,app}}$  obtained from  
 1252  $\ln \frac{c' - c'_{e,app}}{c'_1 - c'_{e,app}}$  versus  $\ln \frac{c - c_{e,app}}{c_1 - c_{e,app}}$ .

(a)	$F_n$ (nmol m <sup>-2</sup> s <sup>-1</sup> )	$v_d$ (cm s <sup>-1</sup> )	$\alpha_{\text{soil}}$	Error $\alpha_{\text{soil}}$	soil cover
SPU-1	-30.1	0.20	0.924	0.032	D. fir, moss
SPU-2	-35.3	0.22	0.948	0.028	D. fir, needles
SPU-3	-37.7	0.20	0.945	0.008	D. fir, moss
SPU-4	-26.1	0.16	0.913	0.004	D. fir, moss
SPU-5	-24.9	0.16	0.918	0.006	D. fir, moss
SPU-6	-13.2	0.12	0.951	0.031	D. fir, moss
SPU-7	-19.6	0.12	0.939	0.005	beech, leaves
SPU-8	-28.4	0.16	0.955	0.008	<i>Same subsite as SPU-7, leaves removed</i>
SPU-9	-20.4	0.12	0.925	0.002	beech, leaves
SPU-10	-22.3	0.13	0.949	0.060	spruce, moss
SPU-11	-19.4	0.13	0.936	0.068	spruce, needles
SPU-12	-40.5	0.28	0.947	0.004	<i>Same subsite as SPU-11, needles removed</i>
MEAN	-26.5	0.17	0.937	/	/

STDEV	8.2	0.05	0.014	/	/
SE	2.4	0.01	0.004	/	/

1253

1254

(b)	$F_n$ (nmol m <sup>-2</sup> s <sup>-1</sup> )	$v_d$ (cm s <sup>-1</sup> )	$\alpha_{\text{soil}}$	Error $\alpha_{\text{soil}}$	soil cover
CBW-5	-6.6	0.04	0.943	0.004	few clover, grass
CBW-7	-3.1	0.03	1.019	0.005	few clover, grass
CBW-16	-22.9	0.18	0.993	0.001	bare soil, few grass
CBW-18	-39.3	0.24	0.950	0.054	grass
CBW-19	-7.4	0.14	0.935	0.105	grass
CBW-20	-14.9	0.20	0.940	0.260	bare soil
CBW-25	-8.0	0.12	0.911	0.014	clover, grass
CBW-26	-6.1	0.09	0.916	0.038	grass
MEAN	-13.6	0.13	0.951	/	/
STDEV	12.2	0.08	0.037	/	/
SE	4.3	0.03	0.013	/	/

1255 Table 2. Net flux, deposition velocity and  $\delta D_{\text{soil}}$  (including error) obtained from the mass  
 1256 balance model for the net  $H_2$  emission experiments.

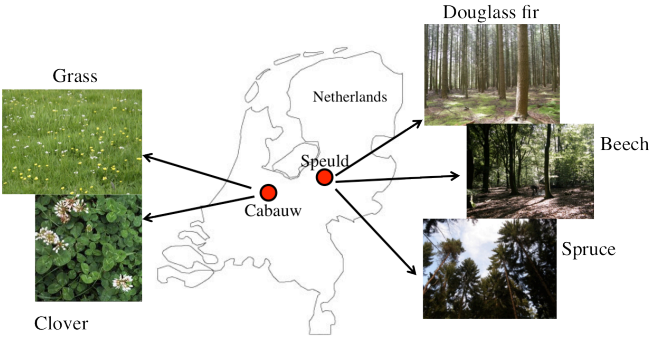
Net emission	$F_n$ (nmol m <sup>-2</sup> s <sup>-1</sup> )	$v_d$ (cm s <sup>-1</sup> )	$\delta D_{\text{soil}}$ (‰)	Error $\delta D_{\text{soil}}$ (‰)
CBW-8	24.5	0.05	-535	53
CBW-10	16.1	0.03	-460	17
CBW-14	13.7	0.02	-629	21
CBW-17	20.3	0.03	-542	1
CBW-21	42.0	0.04	-574	3
CBW-28	150.2	0.14	-488	83
CBW-30	41.0	0.05	-580	7
CBW-31	92.0	0.09	-509	7
CBW-33	46.2	0.10	-451	52
MEAN	49.5	0.06	-530	/
STDEV	44.7	0.04	59	/
SE	14.9	0.01	20	/

Table 3. Sampling information and the correction coefficients ( $k_{\text{true}}/k_{\text{app}}$ ,  $P_{\text{true}}/P_{\text{app}}$ ,  $\alpha_{\text{soil,true}}/\alpha_{\text{soil,app}}$  and  $(\delta D_{\text{soil,true}}+1)/(\delta D_{\text{soil,app}}+1)$ ) used for each experiments. Size S refers to small chamber and size L refers to large chamber.

Exp.	Pressure (kPa)	Flow rate (L min <sup>-1</sup> )	Size	$\Delta t$ (min)	$k_{\text{app}}$ (min <sup>-1</sup> )	$P_{\text{app}}$ (ppb min <sup>-1</sup> )	$k_{\text{true}}/k_{\text{app}}$	$P_{\text{true}}/P_{\text{app}}$	$\alpha_{\text{soil,true}}/\alpha_{\text{soil,app}}$	$(\delta D_{\text{soil,true}}+1)/$ $(\delta D_{\text{soil,app}}+1)$
SPU-1	200	2	S	10	0.199	4.12	1.494	1.601	0.984	/
SPU-2	200	2.2	S	5	0.206	0.67	1.589	7.472	0.998	/
SPU-3	200	3.1	S	5	0.204	3.58	1.496	2.475	0.999	/
SPU-4	200	2.8	S	5	0.160	7.51	1.526	2.136	1.004	/
SPU-5	200	2.6	S	5	0.156	4.16	1.546	2.759	1.004	/
SPU-6	160	3.2	L	5	0.232	7.61	1.184	1.446	0.999	/
SPU-7	160	3.2	S	5	0.128	5.40	1.418	2.264	1.006	/
SPU-8	160	2.5	S	5	0.172	4.23	1.438	2.381	1.001	/
SPU-9	160	2.8	S	5	0.128	4.56	1.440	2.513	1.007	/
SPU-10	180	2.7	S	5	0.128	/	1.502	/	1.005	/
SPU-11	160	2.2	S	5	0.130	/	1.490	/	1.006	/
SPU-12	180	2.3	S	5	0.272	11.30	1.529	1.720	0.994	/
CBW-5	200	2	L	10	0.086	18.24	1.204	1.248	1.001	/
CBW-7	200	1.9	L	10	0.048	11.57	1.260	1.361	0.999	/
CBW-16	210	2.1	S	10	0.183	45.21	1.498	1.505	0.999	/
CBW-18	200	2	S	10	0.240	38.07	1.532	1.527	0.986	/
CBW-19	200	2	S	10	0.145	56.69	1.457	1.463	0.991	/
CBW-20	200	2	S	10	0.196	65.81	1.491	1.494	0.988	/
CBW-25	200	2	S	10	0.122	44.85	1.449	1.460	0.994	/
CBW-26	200	2	S	10	0.088	31.05	1.452	1.475	1.002	/
CBW-8	200	2	S	10	0.044	82.92	1.542	1.438	/	1.048

CBW-10	200	2.6	L	10	0.069	111.00	1.177	1.152	/	1.010
CBW-14	200	2.5	L	10	0.035	82.53	1.251	1.166	/	1.042
CBW-17	220	2.1	L	10	0.047	117.40	1.268	1.198	/	1.024
CBW-21	220	2	L	10	0.078	232.20	1.209	1.179	/	1.008
CBW-28	175	1.8	S	10	0.146	440.90	1.412	1.402	/	1.018
CBW-30	200	2	L	10	0.090	237.70	1.202	1.180	/	1.008
CBW-31	200	2	S	10	0.098	275.10	1.451	1.422	/	1.007
CBW-33	200	2	S	10	0.107	166.50	1.449	1.430	/	1.007

1268 **Figures**



1269  
1270 Fig. 1. The location of the two sampling sites (Cabauw and Speuld) in the Netherlands, as  
1271 well as the plant species there.

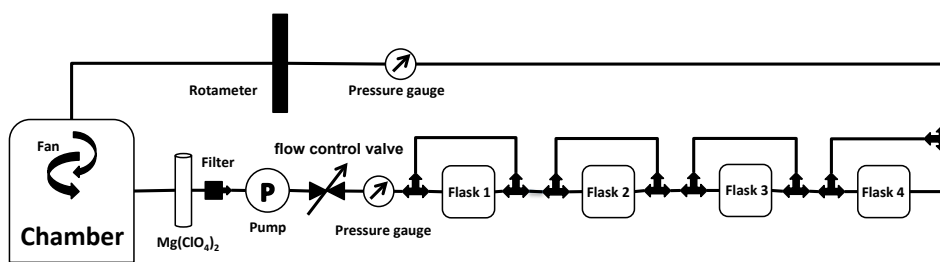
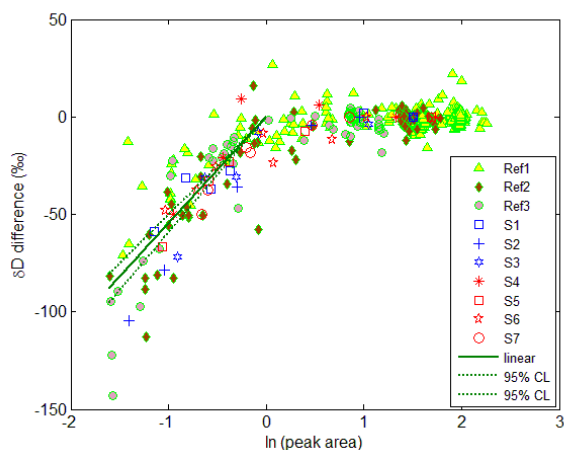


Fig. 2. Scheme of the sampling setup using the closed-cycle air sampler. The volume of the soil chamber was 22.8 L and the volume of each flask was 1 L.





1304

1305 Fig. 3. Difference of  $\delta D$  from the assigned value for different gases including reference gases  
 1306 (Ref1-3) and laboratory flask samples (S1-7). A linear function ( $y = 54.6x$ ) was fit to the data  
 1307 with peak area between 0.2 and 1.0 V s (green solid line; the dashed lines represent the 95%  
 1308 confidence interval of the fit). This function was used to correct the soil experiment data that  
 1309 were measured at low peak areas.

1310

1311

1312

1313

1314

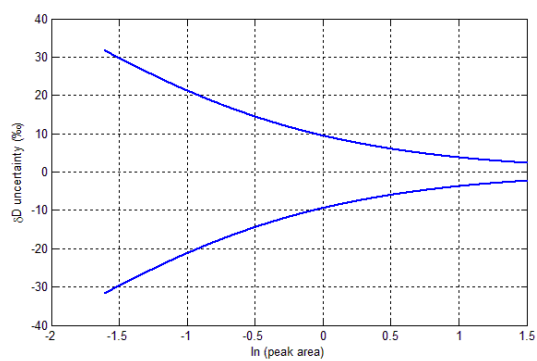
1315

1316

1317

1318

1319



1320

1321 Fig. 4. Calculated total assigned uncertainty of  $\delta D$  (consisting of analytical uncertainty and  
 1322 uncertainty arising from the linearity correction) for air samples with  $\ln(\text{peak area})$  ranging  
 1323 from -1.6 to 1.5.

1324

1325

1326

1327

1328

1329

1330

1331

1332

1333

1334

1335

1336

1337

1338

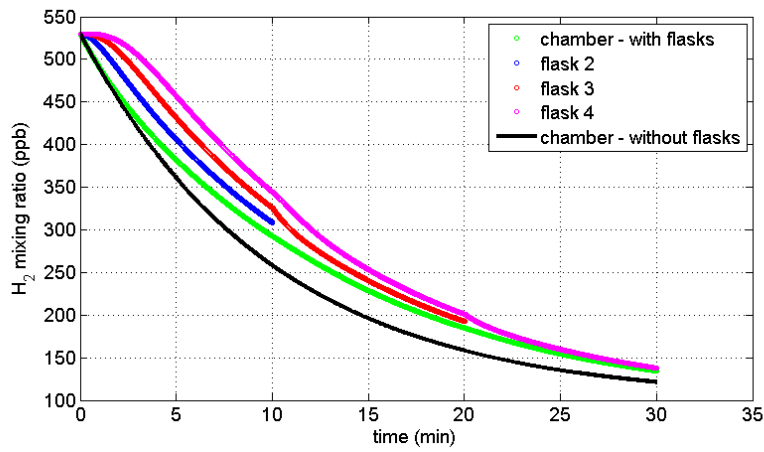


Fig. 5. Results of the flask sampling model with the following parameters:  $k=0.1 \text{ min}^{-1}$ ,  $P=10 \text{ ppb min}^{-1}$  and  $c_1(t=0)=530 \text{ ppb}$ . The figure shows the evolution of  $\text{H}_2$  mole fraction in the chamber (green curve), in flask 2 (blue curve), flask 3 (red curve) and flask 4 (magenta curve) as a function of time, and what would be expected for a chamber without flasks (black curve). Flask 1 was closed before closing the chamber (at time 0 when all volumes contained the same air).

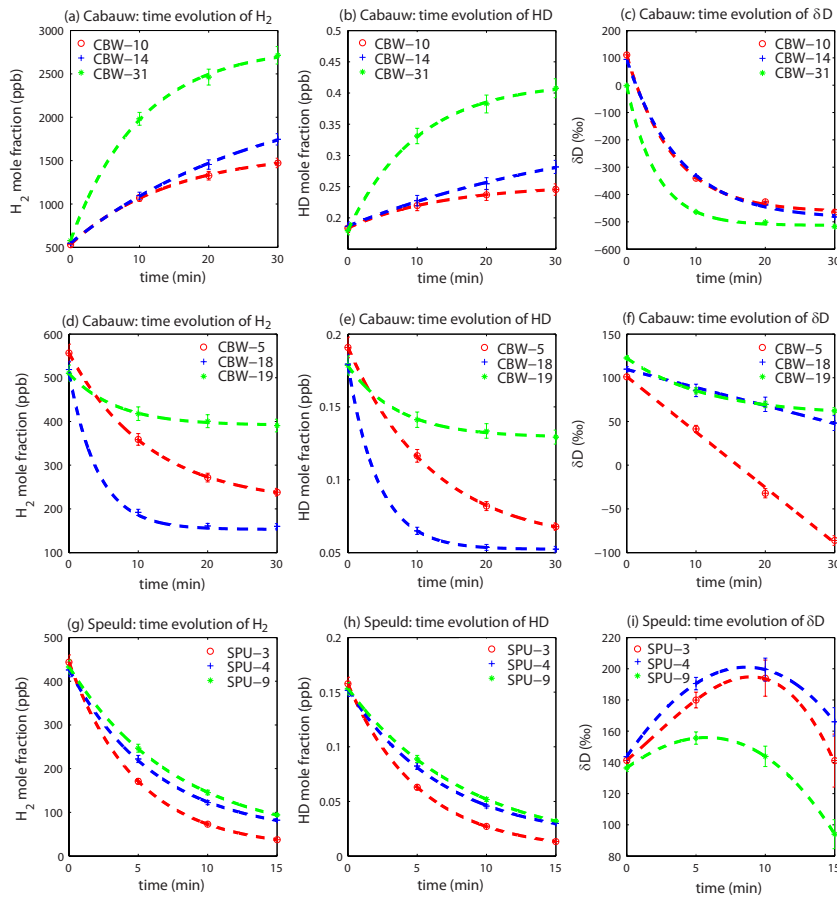
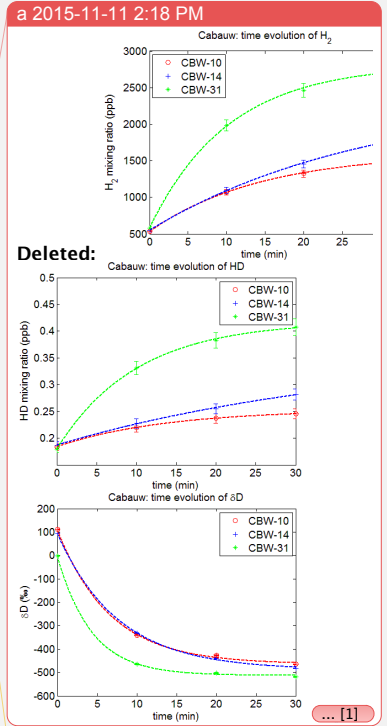


Fig. 6. Time evolution of  $H_2$ , HD and  $\delta D$  in Cabauw (upper and middle panels) and in Speuld (lower panel) for representative experiments. HD is calculated from  $H_2$  and  $\delta D$ . The  $H_2$  data are fitted with an exponential function of the form:  $c = (c_1 - c_{e,app})e^{-k_{app}t} + c_{e,app}$ , where  $c_1$  and  $c_{e,app}$  are the  $H_2$  mole fractions initially and in equilibrium, and  $k_{app}$  is the apparent soil uptake rate constant for  $H_2$ . A similar exponential function is applied to the HD data. Error estimates for  $H_2$ , HD and  $\delta D$  are shown. The connecting lines for  $\delta D$  data are included to guide the eye.

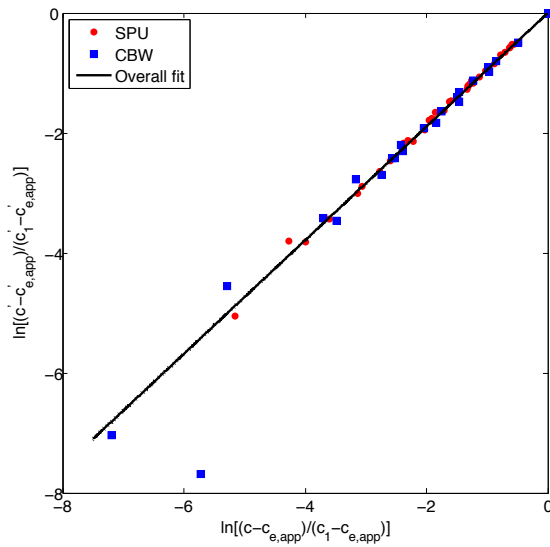
Unknown  
Formatted: Font:Times



Unknown  
Formatted: Font:Times

Unknown  
Formatted: Font:Times

1369  
1370



1371

1372 Fig. 7. Plot of  $\ln \frac{c' - c'_{e,app}}{c_1 - c'_{e,app}}$  versus  $\ln \frac{c - c_{e,app}}{c_1 - c_{e,app}}$  for all Speuld and Cabauw net-uptake  
1373 experiments. The slope of the linear fit to the data returns the fractionation factor  
1374  $\alpha_{soil,app} = 0.947 \pm 0.004$  (95% CI). Errors in x and y direction for each data point were  
1375 considered. One outlier (“CBW-18”) was not included in the fitting. The 95% confidence  
1376 intervals of the fit line are included as dashed lines but largely overlap with the fit line.

1377

1378

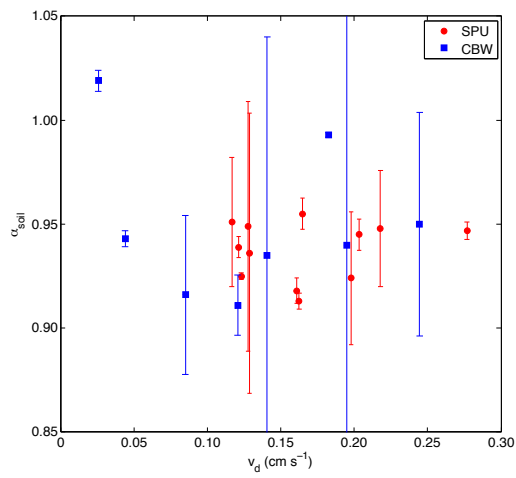
1379

1380

1381

1382

1383  
1384



1385  
1386 Fig. 8. Correlation between  $\alpha_{\text{soil}}$  and  $v_d$  for all Speuld experiments and Cabauw net-uptake  
1387 experiments. The errors for  $\alpha_{\text{soil}}$  were taken from Table 1.

1388  
1389  
1390  
1391  
1392  
1393  
1394  
1395  
1396  
1397  
1398  
1399

1400  
1401  
  
1402  
1403  
1404  
1405  
1406  
1407  
1408  
1409  
1410  
1411  
1412  
1413  
1414  
1415  
1416  
1417  
1418  
1419

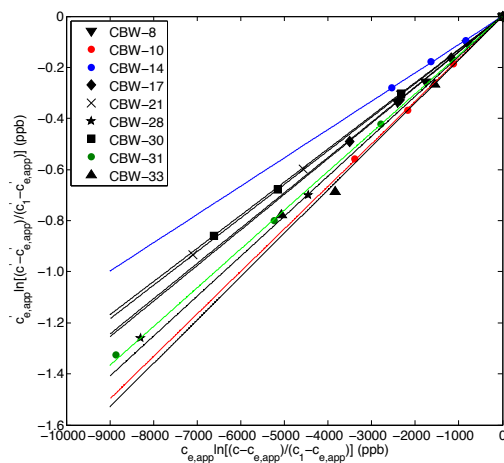


Fig. 9. Plot of  $c'_{e,app} \ln \frac{c' - c'_{e,app}}{c'_1 - c'_{e,app}}$  versus  $c_{e,app} \ln \frac{c - c_{e,app}}{c_1 - c_{e,app}}$  for 9 Cabauw net-emission experiments. A linear function was fit to each individual dataset and the slope was used to calculate the  $\delta D_{soil,app}$  value for each experiment. Errors in x and y direction for each data point were considered.

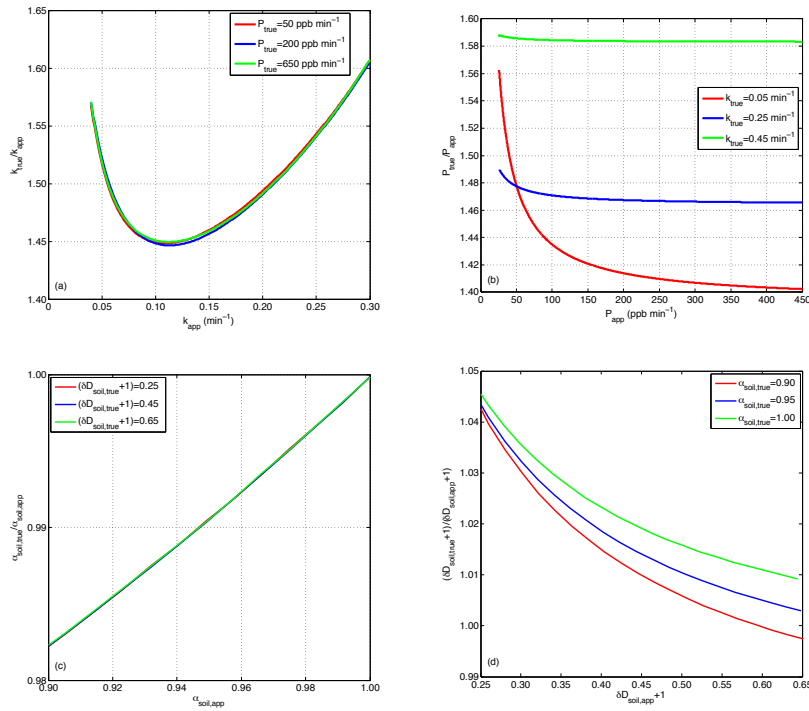


Fig. 10. (a) The relationship between  $k_{\text{true}}/k_{\text{app}}$  and  $k_{\text{app}}$  for  $P_{\text{true}}$  of 50, 200 and 650 ppb min $^{-1}$ ; (b) between  $P_{\text{true}}/P_{\text{app}}$  and  $P_{\text{app}}$  for  $k_{\text{true}}$  of 0.05, 0.25 and 0.45 min $^{-1}$ ; (c) between  $\alpha_{\text{soil,true}}/\alpha_{\text{soil,app}}$  and  $\alpha_{\text{soil,app}}$  for  $(\delta D_{\text{soil,true}}+1)$  of 0.25 to 0.65 for  $k_{\text{true}}=0.25$  min $^{-1}$  and  $P_{\text{true}}= 50$  ppb min $^{-1}$ ; (d) between  $(\delta D_{\text{soil,true}}+1)/(\delta D_{\text{soil,app}}+1)$  and  $(\delta D_{\text{soil,app}}+1)$  for  $\alpha_{\text{soil,true}}$  of 0.90 to 1.00 for  $k_{\text{true}}=0.25$  min $^{-1}$  and  $P_{\text{true}}= 50$  ppb min $^{-1}$ . The parameters of the sampling setup are  $V' = 22.8$  L,  $f=2$  L min $^{-1}$ ,  $\Delta t=10$  min and the pressures inside the flasks and chamber are 200 kPa and 100 kPa respectively.